

# Harnessing Synergies between Combinatorial Microfluidics and Machine Learning for Chemistry, Biology, and Fluidic Design

Suyash S. Damir, Julie Probst, Andrew deMello,\* and Stavros Stavrakis\*

Combinatorial microfluidic systems (CMFs), including droplet-based platforms, concentration gradient generators, and valve-based architectures, enable systematic and high-throughput exploration of complex experimental spaces. These platforms generate large, multidimensional datasets at speeds and scales beyond the capacity of conventional methods. Machine learning (ML) represents a powerful way of analyzing these datasets, uncovering hidden patterns, and guiding experiments through real-time, adaptive control. This review explores the synergistic interaction between CMFs and ML, driving the development of intelligent platforms for chemical synthesis and reaction optimization, biological assays, and microfluidic device design.

Emphasis is placed on closed-loop platforms where ML actively informs experimental decisions, improving speed, precision, and reproducibility. We discuss key challenges to broader adoption, including the limited scalability of microfluidic hardware, the need for standardized, high-quality datasets, and the interpretability of complex ML models. Finally, the importance of interdisciplinary collaboration among engineers, biologists, chemists, and data scientists is highlighted, alongside the development of modular design tools, curated data resources, and explainable artificial intelligence (AI). Together, these efforts are essential to realizing autonomous, ML-driven CMF platforms capable of transforming healthcare, chemical research, and industrial innovation.

## 1. The Marriage of Combinatorial Microfluidics and Machine Learning


Since its advent in the 1980s, microfluidics has revolutionized chemical and biological experimentation by enabling precise control of fluids on the microscale.<sup>[1,2]</sup> This has been driven by the unique capabilities of microfluidic systems when handling small assay volumes. Such capabilities include the creation and homogenization of solute and temperature gradients on ultra-short timescales, and the ease with which complex, multi-step processes can be performed in an integrated fashion. Such features have enabled significant advancements across diverse fields including drug discovery,<sup>[3]</sup> cellular analyses,<sup>[4]</sup> DNA and RNA sequencing,<sup>[5]</sup> organ-on-a-chip technologies,<sup>[6]</sup> point-of-care diagnostics,<sup>[7]</sup> (bio)material synthesis,<sup>[8]</sup> microreactors,<sup>[9]</sup> chemistry,<sup>[10]</sup> and reaction optimization.<sup>[11]</sup>


Microfluidic technologies offer the experimentalist a range of capabilities that are challenging to recapitulate on the large scale. These include precise fluid manipulations, such as mixing,

metering, dilution, incubation, splitting, and separation. When replicated and implemented in parallel, these operations enable multiplexed workflows with high analytical throughput, offering a fluidic analog to semiconductor scaling through microfluidic large-scale integration (mLSI).<sup>[12,13]</sup> Within this rich landscape of scalable fluid control, combinatorial microfluidics has emerged as a powerful approach. For screening and optimization purposes, the term “combinatorial” has traditionally been used to describe mixing of reagents in different proportions.<sup>[14–16]</sup> Herein, we adopt a broader definition. Specifically, a combinatorial microfluidic system (CMF) is defined as any microfluidic workflow designed to systematically explore high-dimensional experimental spaces, by generating and analyzing a wide range of combinations derived from different experimental conditions. In this sense, CMFs encompass three core architectures: droplet-based microfluidics, concentration gradient generators, and valve-based systems (**Figure 1**). These platforms allow for the rapid generation of large, high-quality datasets, accessing throughputs and scalability that far surpass those of conventional bench-top methods. The key strength of CMFs lies in their capacity to integrate units that can act as concentrators or dilutors,<sup>[17–20]</sup> perform combinatorial mixing,<sup>[21–26]</sup> and compartmentalize material within a partition.<sup>[27–29]</sup> These fluidic functions can be automated using various active or passive strategies, such as surface tension driven pumping,<sup>[30]</sup> microfluidic latches,<sup>[13]</sup> and microelectromechanical valves.<sup>[31]</sup> Unsurprisingly, CMFs are widely used in applications such as clinical diagnostics<sup>[32]</sup> and biomarker discovery,<sup>[33]</sup> drug screening,<sup>[23]</sup> single-cell analysis,<sup>[34]</sup> biological synthesis,<sup>[26]</sup> and material synthesis.<sup>[35]</sup>

The automation of CMFs has significantly increased our capacity to generate large, multidimensional datasets by

S. S. Damir, J. Probst, A. deMello, S. Stavrakis  
 Department of Chemistry and Applied Biosciences  
 Institute for Chemical and Bioengineering  
 ETH Zürich  
 Vladimir-Prelog-Weg 1, 8093 Zürich, Switzerland  
 E-mail: andrew.demello@chem.ethz.ch  
 stavros.stavrakis@chem.ethz.ch

 Supporting information for this article is available on the WWW under <https://doi.org/10.1002/cmtd.202500069>

 © 2025 The Author(s). Chemistry - Methods published by Chemistry Europe and Wiley-VCH GmbH. This is an open access article under the terms of the Creative Commons Attribution License, which permits use, distribution and reproduction in any medium, provided the original work is properly cited.

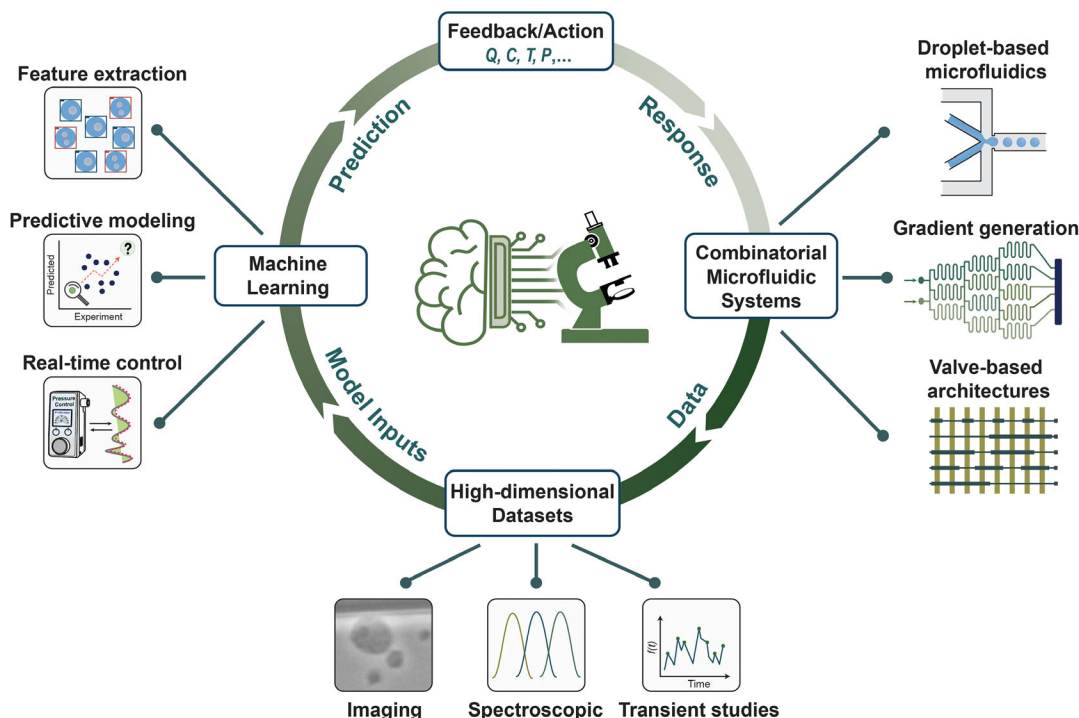


**Figure 1.** Closed-loop optimization strategy harnessing synergies between CMFs and ML promotes development of intelligent microfluidic workflows. Q: flow rate, C: concentration, T: temperature, P: pressure.

enabling high-throughput and reproducible experimentation across many conditions. However, the downstream processing of this data remains a significant bottleneck. Traditional statistical approaches often rely on a priori assumptions, such as fixed error distributions or predefined probabilistic models, and frequently depend on human intervention and intuition—all of which

can introduce bias and reduce reproducibility. A good example in this regard is the heavy reliance on *p*-values whose computation requires subjective choices by the experimenter and whose interpretation can vary significantly across datasets.<sup>[36]</sup> Further, as data volume grows, manual inspection or classification of large-scale datasets such as droplet images or multivariate assay results



**Suyash S. Damir** received his master's degree in chemical and Bioengineering from ETH Zürich in 2024. He is currently working on Triplet-Triplet Annihilation Upconversion (TTA-UC) microcapsules for photocatalytic applications, and integration of analytical techniques into droplet-based microfluidic platforms for probing chemical reactions in-situ.



**Julie Probst** received a PhD degree from the deMello lab at ETH Zürich in 2022. Her thesis focused on droplet-based microfluidic platforms for in situ optical monitoring of fast reactions. She is currently a senior scientist-microfluidic hardware engineer at Anthology, Massachusetts.



**Andrew deMello** is currently Professor of Biochemical Engineering in the Department of Chemistry and Applied Biosciences at ETH Zürich. He obtained a PhD in Molecular Photophysics from Imperial College London (1995) and subsequently held a postdoctoral fellowship in the Department of Chemistry at the University of California, Berkeley, working under Professor Richard Mathies. His group's research interests include the development of microfluidic devices for high-throughput biological and chemical analysis, ultra-sensitive optical detection techniques, and novel methods for nanoparticle synthesis.



**Stavros Stavrakis** received his B.Sc. in Chemistry from the University of Crete in 1999 and his Ph.D. in Biophysical Chemistry there in 2005, specializing in time-resolved vibrational spectroscopy of cytochrome oxidases. He was a Marie Curie fellow at Stanford University and the University of Dundee, working on optical tools for DNA sequencing and optical trapping of single cells. Since 2011, he has been a Senior Scientist and Lecturer at ETH Zurich, focusing on developing advanced microfluidic and optofluidic technologies for biological applications.

becomes increasingly impractical. Altogether, conventional data processing approaches are generally slow and computationally inefficient and fail to capture the full complexity of the datasets produced from combinatorial experiments.<sup>[37,38]</sup>

The advent of machine learning (ML) has fundamentally shifted the paradigm of data processing and analysis.<sup>[39]</sup> Moving away from traditional inference-driven statistical methods, ML emphasizes data-driven learning to uncover patterns and make predictions with minimal assumptions about the underlying data-generating processes. Advancements in the semiconductor industry, marked by continuous reductions in the size and cost of electronic components, have substantially boosted computing power. This progress has enabled the widespread adoption of graphics processing units (GPUs), which allow highly parallelized computation that is well-suited for training complex ML models on large datasets. Combined with the scalability and accessibility of cloud computing, such developments have made it possible to perform computationally demanding tasks with unprecedented efficiency. As a result, neural networks<sup>[40]</sup> and other ML architectures can now tackle complex challenges, such as image recognition<sup>[41]</sup> and natural language processing,<sup>[42]</sup> delivering speed and accuracy far beyond what was previously possible. Through its ability to identify predictive patterns in complex datasets, machine learning has found significant utility in the chemical and biological sciences for a range of applications, from predicting the activity of potential drug candidates<sup>[43]</sup> and planning chemical synthesis experiments<sup>[44]</sup> to predicting protein structure<sup>[45]</sup> and identifying biomarkers.<sup>[46]</sup>

Currently, most ML-assisted microfluidic workflows have primarily employed ML for postexperiment data analysis, aiding in the extraction of insights and optimization of experimental conditions.<sup>[47]</sup> While this approach helps address the limitations of traditional data handling, ML's key strength lies in its ability to uncover latent correlations and features. ML offers a dynamic, adaptive framework that not only assesses system performance in real-time but also iteratively refines its predictions to improve experimental outcomes. When integrated into microfluidic platforms, ML can handle the volume, variety, and velocity of "big data" generated during experiments, enabling real-time decision-making and programmability.<sup>[48]</sup> This in turn reduces the reliance on manual intervention and enables systems to update strategy based on current performance and evolve autonomously, albeit within constraints set by the researcher.

Advances in computer-aided hardware design and microfabrication techniques have markedly reduced the characteristic dimensions of CMFs, enabling hundreds of assays to be conducted in parallel on a single device. For instance, Standard BioTools Inc.'s 96 × 96 dynamic array integrates more than 25,000 valves on a single integrated chip to perform up to 9216 polymerase chain reactions (PCR) simultaneously—generating over 20 times the data of a 384-well plate.<sup>[49]</sup> Concurrently, advancements in machine learning have advanced apace. A striking example is DeepMind's AlphaFold, which progressed from predicting high-confidence structures for 350,000 protein sequences to generating structural predictions for nearly the entire UniProt database (≈200 million entries), with an accuracy comparable to experimental methods, such as X-ray

crystallography and cryo-electron microscopy.<sup>[50–52]</sup> Naturally, the marriage of CMFs and ML is expected to pave the way for autonomous, self-driving laboratories that can analyze, interpret, and optimize complex experimental workflows with minimal human intervention. This synergy has the potential to accelerate experimental cycles and enable high-throughput, data-rich chemical and biological research.<sup>[53]</sup>

Despite significant growth in utilizing both microfluidic technologies and ML for chemical and biological applications, research studies explicitly focused on their synergy remain rare. A literature survey based on selective keywords covering both fields (in Web of Science repository) shows that less than 1% of microfluidics publications since the early 2000s address this synergy (Figure 2, S2, Supporting information). This gap is partly due to the slow evolution of early ML models, which were initially limited to basic pattern recognition and regression tasks and lacked the capacity to handle high-dimensional unstructured datasets. It was not until the early 2000s, with the maturation of neural networks, that ML began to transition from knowledge-driven (rule-based) models to data-driven approaches.<sup>[54–57]</sup> Subsequently, the rise of deep learning in the 2010s enabled ML to process complex multidimensional datasets and make adaptive predictions, stimulating a growing number of studies exploiting synergies between CMFs and ML across a variety of domains. Today, this synergy is leveraged in diverse applications, including nanomaterial synthesis,<sup>[58,59]</sup> microfluidic chip design,<sup>[60]</sup> droplet classification and analysis,<sup>[61,62]</sup> organoids characterization,<sup>[63]</sup> neurotoxicity evaluation of drugs,<sup>[64]</sup> and directed evolution.<sup>[65]</sup>

The primary aim of this review is to discuss how a seamless integration of CMFs and ML is driving the development of programmable, high-throughput experimentation in chemical and biological research, achieving multiplicative, rather than incremental gains. While previous reviews have discussed the use of 'intelligent microfluidics' in the context of biosensors,<sup>[66]</sup> biotechnology,<sup>[67]</sup> design optimization,<sup>[68]</sup> biocatalysis,<sup>[69]</sup> material

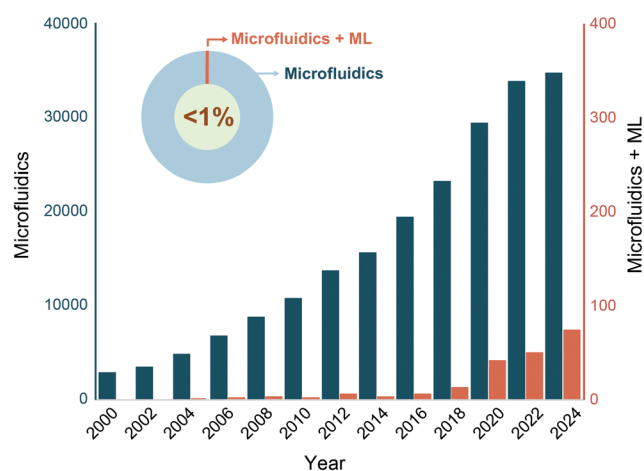


**Figure 2.** Annual publication trends showing the rapid growth of "microfluidics" research (left axis) and the comparatively small but increasing subset of microfluidics publications involving ML (right axis). As of 2024, combined "ML and microfluidics" publications account for less than 1% of all "microfluidics" literature (see donut chart inset). Refer to supporting information for keywords and data.

synthesis,<sup>[8,70]</sup> and organ-on-chip technologies,<sup>[47]</sup> this article takes a different approach. Herein, we focus our discussion on studies that leverage synergies between CMFs and ML to build autonomous systems requiring minimal manual intervention. Rather than treating ML as a passive, postexperimental analysis tool, the emphasis here is on closed-loop systems where ML algorithms direct, optimize, and adapt experiments on-the-fly, thus transforming the experimental workflow. Following a brief overview of the core architectures of CMFs and an introduction to commonly used ML algorithms, we explore how their synergy is advancing three major domains: material synthesis and reaction optimization, biological applications, and microfluidic system design. Finally, we discuss the key challenges involved in developing such integrated platforms and propose solutions, ranging from improved hardware-software integration to interdisciplinary collaboration across engineering, biology, chemistry, and data sciences, that are essential for transitioning these technologies from laboratory prototypes to real-world, deployable systems.

## 2. Combinatorial Microfluidics

### 2.1. Droplet-Based Microfluidics

Droplet-based microfluidic systems allow for the rapid and precise generation of submicroliter droplets at kilohertz frequencies. Importantly, their submillisecond mixing capabilities, along with efficient heat and mass transfer, and the exquisite control over reagent payloads make them particularly well suited for exploring vast sets of distinct reaction conditions in a high-throughput manner.<sup>[71]</sup> A representative example in this regard is a combinatorial sample preparation platform developed by Samimi and coworkers.<sup>[72]</sup> This system is capable of generating droplets with bespoke reagent compositions, performing on-demand mixing of up to eight reagent plugs into a single, homogeneous sample plug. This plug is then emulsified into picoliter droplets. Optical barcoding of droplets is achieved by delivering different dye combinations into each droplet, creating a coding space of up to 169 unique barcodes, each representing a distinct experimental composition. The authors validated the platform by constructing a 25-condition library for antibiotic susceptibility testing of *E. coli*, successfully identifying minimum inhibitory concentrations (MICs) across multiple antibiotics and concentration gradients in a single experiment. Building on this concept, Cao et al. combined a programmable formulator, capable of generating custom reagent-substrate combinations, with a T-junction droplet generator.<sup>[73]</sup> Here, droplets were generated in pairs, one containing a specific reagent concentration and the other an enzyme introduced *via* a secondary inlet. Subsequent sequential droplet merging allowed the testing of up to 32 different conditions per experiment run.

As another example, Bawazer and coworkers investigated over 100 combinations of oils and surfactants against an aqueous titanium salt solution to find conditions that yielded droplets with enhanced stability (Figure 3a).<sup>[35]</sup> The experimental setup utilized a commercial vacuum manifold connected to 24 parallel

polydimethylsiloxane (PDMS) droplet generators, enabling high-throughput screening. To efficiently navigate the vast parameter space, the team employed a genetic algorithm. The algorithm served as a computational optimization method that iteratively refined solutions based on performance metrics. This approach resulted in a 10-fold increase in screening throughput compared to conventional methods.<sup>[74,75]</sup> The authors validated their approach by demonstrating improved droplet stability during protein expression and analysis, underscoring the practical value of the screening strategy for generating stable droplets in biological assays. It should also be noted that these findings are broadly applicable to various microfluidic applications ranging from DNA amplification<sup>[76]</sup> and single-cell analysis<sup>[77]</sup> to polymerization<sup>[78]</sup> and catalysis.<sup>[79]</sup>

### 2.2. Gradient Generation

Biological systems are inherently dynamic, with cellular responses often modulated by gradients in the extracellular environment through intricate signaling pathways. Over the years, many technologies have been developed to generate concentration gradients, particularly for *in vitro* studies of cellular behavior.<sup>[80,81]</sup> CMFs allow precise and stable concentration gradient generation of multiple reagents in parallel, owing to their superior spatial and temporal control. This capability has been critical in numerous applications, including the investigation of cellular responses to varying drug concentrations,<sup>[20]</sup> the analysis of enzyme kinetics,<sup>[82]</sup> the assessment of toxicity,<sup>[83,84]</sup> and the study of cancer cell chemotaxis.<sup>[85]</sup>

A number of recent studies highlight the versatility of microfluidic gradient generation. In one study, Nguyen and coworkers reported a ladder-shaped microfluidic system for rapid antibiotic susceptibility testing (Figure 3b).<sup>[86]</sup> The system employed a passive dilution strategy to achieve two-fold serial dilutions at each loop, accommodating clinically relevant antibiotic combinations. The method demonstrated over 90% agreement with standard methods when determining the MIC of bacteria isolated from urinary tract infections. Beyond liquid-phase gradients, microfluidic systems also support the development of gaseous gradients, enabling the rapid and tunable delivery of oxygen to cells. In one such study, Chang et al. developed a PDMS-polycarbonate (PC) hybrid microfluidic platform capable of simultaneously generating orthogonal chemical and oxygen gradients for cell culture studies.<sup>[87]</sup> This device consists of two PDMS layers, the top layer consisting of spatially confined chemical reactions to generate O<sub>2</sub> gradients and the bottom layer to generate chemical (drug) concentration gradients. These layers are separated by a thin PC film embedded into the top PDMS layer to reduce O<sub>2</sub> diffusion to the atmosphere. For showcase utility, the authors exposed A549 lung carcinoma cells to gradients of tirapazamine (TPZ), a hypoxia-activated prodrug, and systematically evaluated cell viability across zones of varying drug concentration and oxygen tension. Results revealed that TPZ cytotoxicity was significantly enhanced under hypoxic conditions highlighting both the accuracy of gradient generation and the platform's utility in mimicking complex tumor microenvironments.

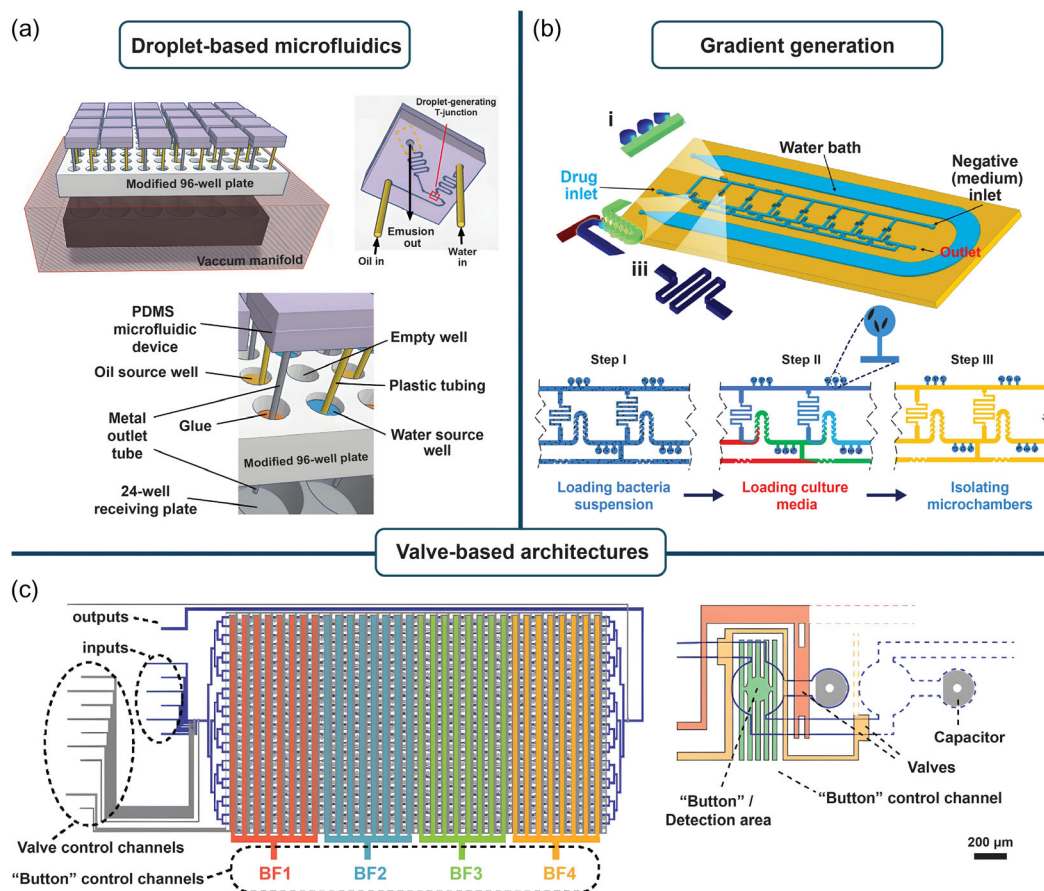


**Figure 3.** Combinatorial microfluidic strategies. a) Droplet-based microfluidics—schematic of 24 parallel PDMS droplet-generators interfaced with a 96-well plate. The setup is mounted on a vacuum manifold to motivate the flow of oil and aqueous inlets through fluidic channels, reproduced with permission.<sup>[35]</sup> Copyright 2016, American Association for the Advancement of Science's (AAAS). b) Gradient generation—on top, schematic of a ladder microfluidic system integrating an on-chip water bath, and below, protocol for platform operation. Reproduced with permission.<sup>[86]</sup> Copyright 2023, Springer Nature. c) Valve-based architectures—schematic overview of the k-MITOMI platform. Blue and gray lines represent flow and control channel, BF1 to BF4 are four button valves. Right section of the panel depicts a typical k-MITOMI unit cell. Reproduced with permission.<sup>[95]</sup> Copyright 2012, National Academy of Sciences.

To further increase the gradient dimensionality, Li et al. used a SlipChip<sup>[88]</sup> platform to create a triple-gradient matrix (three chemicals on a single device) enabling high-throughput protein crystallization studies.<sup>[89]</sup> This 3D matrix allows the screening of over 100 multiparametric conditions in a single experiment, offering cost effectiveness and significantly high screening efficiency compared to existing double-gradient generating platforms. Similarly, in the direction of advancing combinatorial screening capabilities, Toh et al. developed the 3D HepaTox Chip, a microfluidic platform designed for *in vitro* drug hepatotoxicity studies.<sup>[90]</sup> The device integrates a linear concentration gradient generator with a multiplexed cell culture module consisting of eight parallel microchannels, each delivering a distinct drug concentration to a dedicated 3D primary hepatocyte culture. This architecture enabled a simultaneous, dose-dependent administration of multiple drugs to functional hepatocytes within a single experiment. The platform preserved hepatocyte function by maintaining a physiologically relevant 3D microenvironment, while streamlining high-throughput hepatotoxicity screening, bridging the gap between conventional well-plate assays and *in vivo* drug response prediction.

### 2.3. Valve-Based Architectures

Isolating samples or reactions inside discrete microenvironments is a core feature of microfluidic technologies. This allows precise, high-resolution measurements at the single-cell or single-molecule level; capabilities that traditional bulk methods lack, since they provide only averaged population responses.<sup>[91]</sup> In valve-based microfluidic systems, cells or molecules are compartmentalized in micro- to nanoliter wells, chambers, or droplets, facilitating individual analysis and supporting high-throughput, multiplexed experimentation.

Recent developments in multiplexed valve-based architectures have significantly improved the efficiency of cell trapping and single-cell analysis. In a notable example, Maerkl et al. developed MITOMI (Mechanically Induced Trapping of Molecular Interactions), a high-throughput combinatorial platform designed to quantify transient and low-affinity DNA-binding interactions of transcription factors.<sup>[28]</sup> The device, featured 2400 independent unit cells regulated by 7233 valves, enabling the mapping of DNA-binding landscapes of four eukaryotic cells to basic helix-loop-helix transcription factors (TFs). Specifically, it quantified

absolute binding affinities across thousands of permutations involving 464 unique DNA sequences. By capturing weak and transient molecular interactions with high precision, MITOMI overcomes limitations associated with conventional semi-quantitative protein-DNA microarrays<sup>[92,93]</sup> and other methods such as surface plasmon resonance, with the latter being typically constrained by low-throughput.<sup>[94]</sup> Building on this, Geertz et al. introduced k-MITOMI, an adaptation for kinetic measurements that enabled parallel quantification of hundreds of biomolecular association and dissociation rates on a single chip (Figure 3c).<sup>[95]</sup>

In 2014, Fluidigm released the C1 integrated fluidic circuit AutoPrep system, a fully automated microfluidic platform designed for high-throughput single-cell analysis. This system enables efficient isolation, processing, and analysis of up to 96 individual cells in parallel, streamlining workflows for cell capture, lysis, and nucleic acid preparation. Inspired by this platform, several studies adopted similar microfluidic strategies for both targeted and whole-genome analysis in single cells.<sup>[96–98]</sup> For example, Yang et al. developed a microfluidic device containing parallel amplification units and integrated microvalves to trap, lyse, and amplify genomic DNA from individual cells.<sup>[99]</sup> This system trapped individual tumor cells employing microvalves in eight parallel amplification units, where each cell was subsequently lysed and its genomic DNA amplified. This approach achieved over a 1,000-fold amplification from a single cell while significantly reducing reagent usage and operational costs by up to three orders of magnitude compared to traditional pipetting and microtube methods.

Valve-based platforms are also particularly advantageous for combinatorial synthesis, owing to their ability to rapidly generate and screen large libraries. For example, Eduati et al. developed a multiplexed microfluidic platform incorporating Braille valves to screen drug combinations directly on pancreatic cancer patient biopsies.<sup>[24]</sup> Sixteen syringes were used to deliver reagents into the device, while Braille pins enabled rapid switching of fluid streams to generate combinatorial plugs at high throughput. This setup allowed screening of over 1200 data points (fluorescence measurements with multiple replicates) per biopsy, offering a solution when only small quantities of patient cells are available.

## 3. Machine Learning

### 3.1. Common Machine Learning Models in Microfluidics

In basic terms, machine learning refers to algorithms that enable computers to learn from data, uncover patterns, and make predictions or optimize outcomes based on defined performance metrics. A machine learning model is the outcome of training an algorithm on a dataset; it captures the relationship between variables that the algorithm has learned from the data. ML training can be classified into three primary subtypes: supervised learning, unsupervised learning, and reinforcement learning (RL). In supervised learning, the model is trained on labeled data, where each input is paired with a known output, allowing the algorithm to learn the mapping between them. This can take

the form of classification, where the goal is to assign inputs to discrete categories (e.g., distinguishing between two cell types), or regression, where the model predicts continuous numerical values. Unsupervised learning involves training on unlabeled data, where the algorithm autonomously identifies underlying structures, groupings, or patterns without predefined outcomes. RL, inspired by behavioral psychology, trains an agent to make decisions through trial and error, receiving rewards or penalties based on its actions. By integrating supervised learning with dynamic programming, RL focuses on optimizing decision-making over time, minimizing or maximizing long-term rewards rather than simply predicting static outcomes.

**Figure 4** illustrates the most common ML algorithms that have been used in conjugation with microfluidic systems. A decision tree algorithm is a type of supervised learning algorithm and can be used for both classification and regression problems. It structures decisions hierarchically: internal nodes represent features, branches denote decision rules, and leaf nodes indicate outputs. A random forest algorithm extends this approach by combining multiple decision trees, each generating independent predictions, with the final output determined by majority vote. Another supervised learning method, Naïve Bayes, is based on Bayes' theorem and assumes feature independence within a dataset. Despite this simplification, it allows for effective handling of complex problems, even with limited or mislabeled data, reducing the need for large datasets.

Artificial neural networks (ANNs) are computational models inspired by biological neurons, consisting of interconnected artificial neurons organized into input, hidden, and output layers. Each connection between neurons carries a weight that is optimized during training to improve predictions. Deep learning refers to ANNs with many hidden layers (also referred to as deep neural networks, DNNs), which can learn increasingly abstract features from raw data, such as images. This depth allows DNNs to detect subtle patterns that shallower models often miss, making them particularly effective for high-dimensional tasks.<sup>[100]</sup> A specialized class of DNNs, convolutional neural networks (CNNs), excel in image recognition and classification, which are particularly relevant to microfluidic applications. They process data through sequential layers, input, convolution, pooling, flattening, and fully connected, automatically extracting hierarchical features without manual selection. This method enhances visual recognition accuracy while reducing human bias. CNNs are particularly powerful in detecting subtle morphological variations that may be overlooked by human analysis or conventional image processing techniques. Given the wide range of microfluidic applications, spanning materials science, biology, and device engineering, different ML models are better suited for different tasks. **Table 1** summarizes an overview of commonly used ML models in microfluidics, highlighting their strengths, limitations, and representative application areas.

The utility of ML models extends beyond offline image processing to real-time control in microfluidic systems. In closed-loop configurations, CNNs can not only analyze droplet or cell images but also trigger on-the-fly actuation events such as valve switching or sorting based on morphological features.<sup>[101]</sup> Furthermore, RL algorithms, inspired by hippocampal learning processes,<sup>[102]</sup>

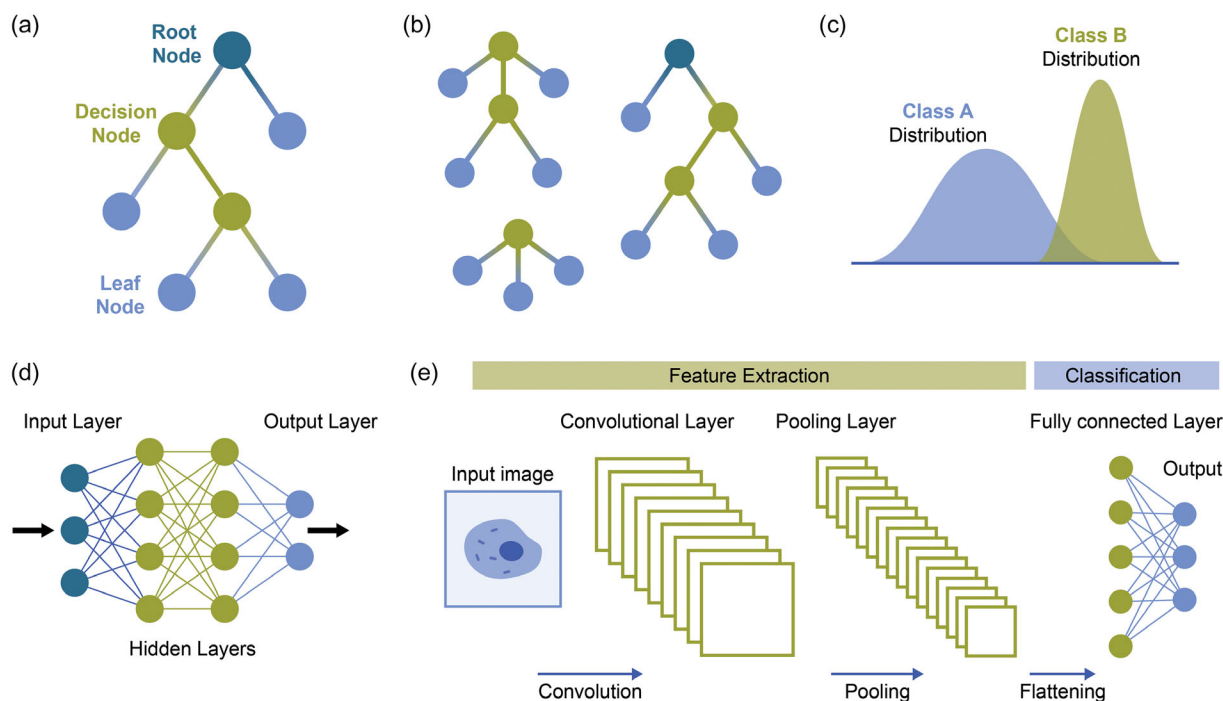


**Figure 4.** Overview of machine learning algorithms commonly integrated with microfluidic systems. a) Decision trees, b) Random forests, c) Naïve Bayes, d) Artificial Neural Network, and e) Convolutional Neural Network.

can optimize control strategies in real-time, such as modulating flow rates or reagent concentrations, through feedback-driven reward systems.<sup>[103]</sup> Together, these models form the computational backbone of closed-loop optimization platforms, enabling microfluidic systems to autonomously adapt to variation, optimize outcomes, and improve operational robustness.

### 3.2. On the Importance of Data

The selection and development of accurate ML models depend on both the quantity and quality of available data. In many applications, such as drug discovery or single-cell analysis, diverse, high-quality datasets are often scarce. This is due in large part to nonstandardized data acquisition protocols and inconsistent experimental readouts (e.g.,  $IC_{50}$ , cell viability, and reaction yield), leading to heterogeneous chemical and biological databases.<sup>[104,105]</sup> Such datasets tend to be biased toward specific interests, defined by the researcher's objectives, resulting in skewed predictions (e.g., calculated reaction yield  $> 100\%$ )<sup>[106]</sup> and a limited domain of applicability.

To address this data imbalance, automated, high-throughput experimentation coupled with standardized protocols can enhance reproducibility across different experiments.<sup>[107]</sup> To this end, large-scale experimental screening is particularly valuable, as it includes both successful and failed outcomes enabling the generation of unbiased datasets. For instance, Lu et al. screened over 10,000 conditions for a photocatalytic [2 + 2] cycloaddition reaction using a liquid-core waveguide microfluidic reactor.<sup>[108]</sup> AI algorithms were employed to deconvolute nonsteady-state absorbance signals from both reacted and unreacted mixtures, generating vast amounts of high-quality data in a short time.

Similarly, Granda et al. used an ML-guided robotic chemical handling system to explore the reaction space of Suzuki–Miyaura coupling.<sup>[109]</sup> They generated a dataset of 3456 reactions through systematically varying reactants, ligands, bases, and solvents to train a neural network for predicting reaction yields. By representing chemical inputs as binary vectors (denoting the presence or absence of reactants), they sampled a chemical reaction space without prior structural or reactivity knowledge, generating a sufficiently diverse and exhaustive dataset for predictive modeling of unexplored reaction combinations. Despite the time and expertise required, meticulous data curation remains essential for constructing standardized datasets that enable accurate ML predictions and reliable interpretation. In this context, CMFs offer a significant advantage by generating reproducible, multidimensional, and broad datasets, making them well-suited for training neural network-based classifiers and other ML models.

## 4. Synergies between Combinatorial Microfluidics and Machine Learning

The growing analytical and predictive capabilities of ML pair seamlessly with the capacity of CMFs to generate high-quality, high-volume data. The pieces fit perfectly. However, leveraging the full potential of both fields requires more than just simple integration. While integration involves employing ML to assist specific experimental or analytical steps, synergy enables a feedback loop where microfluidic experiments and ML decisions complement each other (Figure 1). This approach results in accelerated discovery of novel molecules and therapeutics, enables deeper exploration of complex reaction spaces, and

**Table 1.** Summary of important ML models used in synergy with CMFs.

ML model	Category	Strengths	Limitations	Computational cost for microfluidic tasks	Applications
<b>Decision Trees</b>	Supervised	Simple, interpretable; fast inference; low computational cost	Prone to overfitting; limited with complex, high-dimensional data	Low	Classification of cells and droplet contents; <sup>[211,212]</sup> flow control <sup>[213]</sup>
<b>Random Forests (RF)</b>	Supervised (Ensemble)	Robust to overfitting; handles nonlinearities; good with mixed data types	Slower than single trees; less interpretable	Low-medium	Cell classification; <sup>[214]</sup> biomarker assay analysis; <sup>[211]</sup> organ-on-a-chip <sup>[162]</sup>
<b>Naive Bayes</b>	Supervised	Fast training; works well with small or noisy datasets	Assumes feature independence (often unrealistic); limited to simpler tasks	Very low	Self-optimization of device; <sup>[215]</sup> Object classification in medical datasets <sup>[216,217]</sup>
<b>Artificial Neural Networks (ANNs)</b>	Supervised	Captures complex nonlinear relationships; flexible architecture	Requires large, labeled datasets; training can be slow	Medium-high (depends on architecture size)	Droplet/microparticle size prediction; <sup>[123]</sup> reaction space optimization <sup>[128]</sup>
<b>Convolutional Neural Networks (CNNs)</b>	Supervised (Deep)	Excellent for image data; automates feature extraction; scalable to high-dimensional inputs	Computationally intensive; sensitive to image quality; requires annotated image datasets	High	Image-based droplet sorting; <sup>[4,101,134]</sup> single-cell analysis; <sup>[132,153]</sup>
<b>Reinforcement Learning (RL)</b>	Trial-and-error	Learns optimal control policies; adapts online; ideal for closed-loop systems	Requires many training iterations; reward design is critical; can be unstable	High	Real-time flow control; <sup>[103]</sup> reaction optimization; <sup>[11]</sup>
<b>Support Vector Machines (SVMs)</b>	Supervised	Effective in high-dimensional spaces; good generalization	Difficult to tune; not scalable to very large datasets	Medium	Nanoparticle synthesis optimization; <sup>[58]</sup> binary classification tasks <sup>[212]</sup>
<b>Long Short-Term Memory (LSTM)</b>	Supervised (Deep, Recurrent)	Handles sequential data; good memory of prior states	High computational load; requires careful architecture tuning	High	Temporal analysis of cell trajectories; <sup>[132]</sup> mechanical property estimation <sup>[122]</sup>
<b>Autoencoders</b>	Unsupervised (Deep)	Dimensionality reduction; captures abstract representations of complex inputs	Poor interpretability; may miss rare features	Medium-high	Morphological descriptor extraction <sup>[177]</sup>
<b>Bayesian Optimization</b>	Bayesian	Sample-efficient; handles uncertainty; good for expensive experiments	Struggles with high-dimensional spaces; computational cost scales poorly with dimensions	Medium high	Device design; <sup>[218]</sup> synthesis parameter tuning <sup>[117]</sup>

streamlines multifaceted chemical and biological processes. In the following section, we explore the impact of this synergy across three key domains *viz.*, material synthesis and reaction optimization, biological applications, and enhanced microfluidic design.

#### 4.1. Material Synthesis and Reaction Optimization

Rational chemical synthesis of target molecules and nanoparticles has evolved from a purely human-driven, knowledge-based process to a sophisticated, data-driven approach, powered by collaboration between human expertise and machine intelligence. This endeavor began with the pioneering LHASA project, which sought to streamline organic synthesis through logic-based heuristics.<sup>[110]</sup> Over time, this approach has evolved into ML-guided, high-throughput methods for data-driven material discovery, an approach Pensak and Corey laid the groundwork for in the 1970s.<sup>[111,112]</sup> Today, ML-driven platforms are revolutionizing chemical synthesis, offering predictive insights and accelerating the discovery process beyond traditional heuristic and rule-based methods.

A key application of ML-guided CMFs is the precision synthesis of inorganic nanoparticles (NPs) and metal halide quantum dots (QDs). NP synthesis is a complex multistep chemical optimization problem, as properties such as morphology and optoelectronic behavior are highly sensitive to variables such as reagent concentration, solvent, ligands, temperature, and residence time.<sup>[113]</sup> The key challenge lies in identifying optimal synthesis conditions within a parameter space of continuous and discrete variables. By enhancing experimental throughput and integrating machine learning algorithms, this challenge can be addressed from both hardware and software perspectives.<sup>[114]</sup> Conventional flask-based, trial-and-error approaches are often slow, prone to batch-to-batch variability, and difficult to couple with inline analysis and feedback algorithms. In contrast, microfluidic reactors integrated with ML can rapidly and reproducibly explore vast parameter spaces, enabling self-optimizing workflows that converge on optimal synthesis conditions with far fewer experiments. This has been beautifully exemplified by Bezing and coworkers who coupled the goal-seeking algorithm MARIA (Multiparametric Automated Regression Kriging Interpolation and Adaptive Sampling) with a segmented-flow microfluidic reactor.<sup>[115]</sup> The setup intelligently mapped a 3D parameter space to tune metal composition and achieve target emission characteristics of complex perovskite nanocrystal compositions in far fewer iterations than an exhaustive parametric screening. Similarly, Tao et al. developed a self-driving microfluidic-machine learning (MFML) platform employing the Gryffin algorithm to optimize gold nanoparticle synthesis.<sup>[58]</sup> By systematically varying concentrations, pH, and reaction time and analyzing spectroscopic feedback, the system rapidly identified optimal conditions (Figure 5a–c). In addition to using the Gryffin algorithm for experimental planning, the authors employed supervised learning models, including random forest and support vector regression,<sup>[116]</sup> to predict spectroscopic characteristics of target gold nanoparticles. The approach not only accelerated synthesis but

also offered better interpretability, revealing how different reaction parameters influence nanoparticle properties and demonstrating capabilities of CMFs-ML synergy.

Autonomous, ML-driven microfluidic platforms, such as the 'Artificial Chemist', leverage iterative experimentation and neural network optimization to synthesize bespoke perovskite QDs with high precision and minimal material use (Figure 5d–f).<sup>[117]</sup> Leveraging adaptive sampling and decision-making algorithms, the platform optimized key optoelectronic properties of QDs, including photoluminescence quantum yield, emission linewidth, and peak emission energy, achieving high precision synthesis with minimal material consumption. A neural network-based Bayesian optimization algorithm was implemented, outperforming traditional Gaussian processes<sup>[118,119]</sup> in navigating the halide exchange reaction space of CsPbBr<sub>3</sub> QDs.

Droplet-based microfluidics combined with ML algorithms is transforming the synthesis and analysis of microcapsules and microparticles, where machine learning models are increasingly employed to predict and control key physical characteristics such as droplet size and particle morphology.<sup>[120–123]</sup> For instance, Damiati and coworkers generated micron-sized poly (D, L-lactide-co-glycolide) (PLGA) droplets which resulted in PLGA microparticles upon solvent evaporation.<sup>[123]</sup> To predict droplet and particle sizes across various microfluidic devices, the team developed five ANNs each tailored to a specific microfluidic chip, which were subsequently merged into a unified model. This consolidated ANN streamlined the synthesis workflows, offering cross-platform size prediction and significantly accelerating the optimization process (Figure 6a–d). Similarly, Lin et al. introduced a hybrid ML approach combining a deep convolutional neural network (DCNN) with a long short-term memory (LSTM) network to assess the mechanical properties of microcapsules based on their deformation in branched microfluidic channels.<sup>[122]</sup> This method allowed real-time, high-throughput characterization of thousands of microcapsules per second, outperforming conventional analysis techniques and highlighting the potential for rapid, automated quality control in microfluidic experiments. In the context of pharmaceutical formulations, Su et al. demonstrated how integrating droplet microfluidics with deep learning can streamline the screening and characterization of crystallization conditions for active pharmaceutical ingredients (Figure 6e–h).<sup>[124]</sup> Leveraging the rapid screening capabilities and minimal sample requirements of droplet microfluidics, features especially valuable in early-stage drug development, the authors used hydrogel droplets to grow indomethacin crystals of varying morphologies (e.g., rod, sheet, and wire). Finally, a deep neural network was trained on microscopy data to automate crystal morphology classification, significantly accelerating the screening process and reducing manual analysis times.

Optimizing chemical reactions is a complex task that involves identifying the optimal reagent ratios and reaction conditions to achieve specific outcomes, such as improved yields, faster reaction rates, or precise particle size distributions, all in the least number of steps. Conventional optimization techniques, including one-variable-at-a-time (OVAT) and design of experiments (DoE), though widely used, often suffer from inefficiencies and inconsistent identification of optimal conditions.<sup>[125,126]</sup>

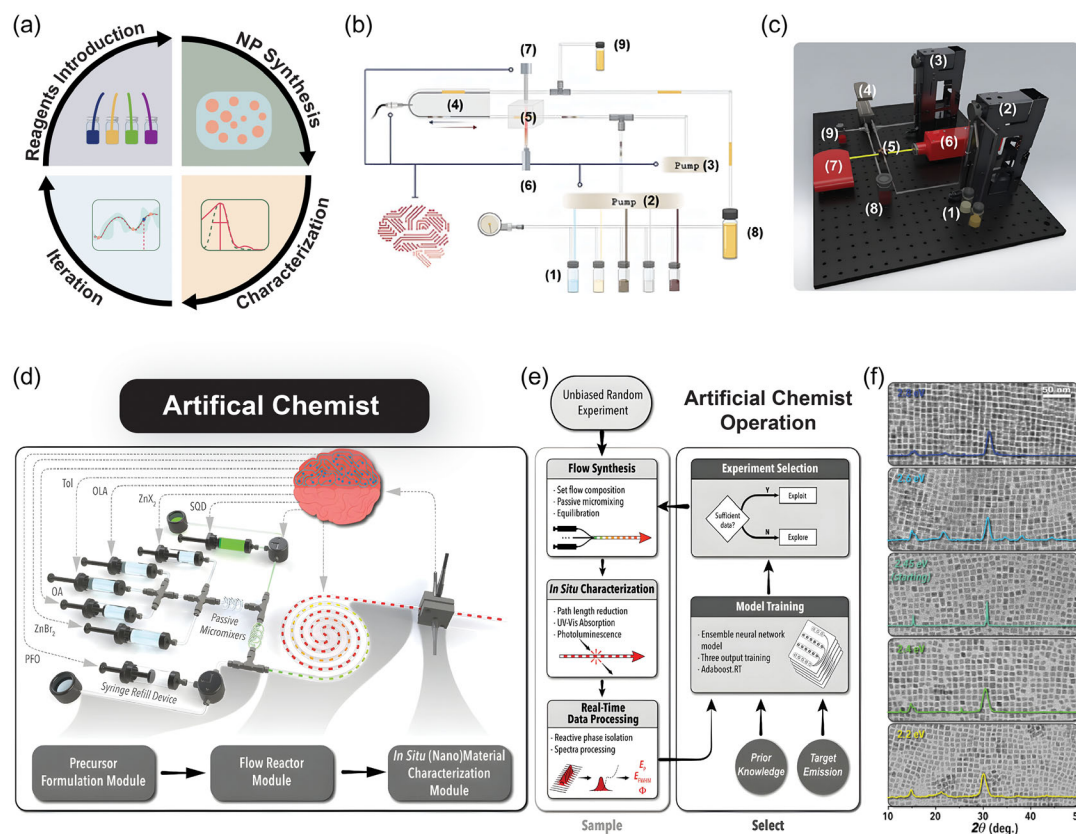


**Figure 5.** Precision synthesis of inorganic nanoparticles (NPs). a) Closed-loop workflow of the self-driving microfluidic-machine learning (MFML) platform for NP synthesis and b) 2D and c) 3D schematic of the MFML platform consisting of (1) reagent solutions, (2) dispenser pump, (3) oscillator pump, (4) oscillatory MF flow reactor, (5) flow cell, (6) light source, (7) spectrometer, (8) waste container, and (9) sample collection outlet. (a–c) Reproduced with permission.<sup>[58]</sup> Copyright 2021, Wiley-VCH. d) Modular microfluidic platform for autonomous QD synthesis with in-situ absorbance and photoluminescence detection, e) process flow diagram of Artificial Chemist's operation, and f) transmission electron microscopy images of the synthesized quantum dots overlaid with X-ray diffraction spectra of the purified halide-exchanged QDs. (d–f) Reproduced with permission.<sup>[117]</sup> Copyright 2020, Wiley-VCH.

Microfluidic systems, with their enhanced fluid control, improved thermal and mass transfer, rapid reaction kinetics, and reduced reagent consumption, offer significant advantages in this context. When combined with ML algorithms, these features enable more efficient navigation of multidimensional reaction spaces, reducing optimization time and improving accuracy.

To this end, Zhou et al. introduced the deep reaction optimizer (DRO), an RL-based framework that interacts with the experimental environment to suggest optimal reaction conditions.<sup>[11]</sup> Using micron-sized droplets as chemical containers, DRO was applied to optimize four organic synthesis reactions, outperforming traditional black-box models such as OVAT and covariance matrix adaptation evolution strategy (CMA-ES) in yield maximization.<sup>[126,127]</sup> The system completed reaction optimization in under 30 min, leveraging both fast reaction kinetics and efficient decision-making algorithms. Impressively, DRO was able to generalize across different reaction types, reducing the number of iterations needed to optimize a new system. In a complementary effort, Rizkin and coworkers designed a continuous-flow microfluidic platform integrated with automated design of experiments, fluid handling, and analytics to study the kinetics of a zirconocene polymerization catalyst.<sup>[128]</sup> By coupling the setup with ANNs and Latin hypercube sampling, a statistical method to explore multidimensional parameter spaces, they

constructed a high-resolution map of the reaction landscape, surpassing capabilities of conventional experimental strategies. The approach offered a holistic optimization framework, factoring in catalytic productivity, energy efficiency, environmental impact, and cost, while simultaneously minimizing chemical waste and accelerating the discovery of optimal reaction pathways.

## 4.2. Biological Applications

Microfluidics has been pivotal in advancing biological research, with early applications dating back to the development of miniaturized gas chromatographs<sup>[129]</sup> and microfabricated capillary electrophoresis systems.<sup>[130]</sup> The ability to manipulate complex microflows in a combinatorial manner has since enabled a broad range of biological applications, from cellular classification<sup>[27,131,132]</sup> and sorting<sup>[133–135]</sup> to bioassay development,<sup>[136,137]</sup> genomic analysis,<sup>[96,98,99]</sup> drug screening,<sup>[3,24,138]</sup> and organ-on-chip platforms.<sup>[139–142]</sup> When combined with ML's ability to process high-dimensional data and extract meaningful biological patterns, microfluidic platforms become even more powerful, enabling faster, more reliable, and information-rich biological experimentation. In this section, we highlight key areas where this synergy is driving significant progress.

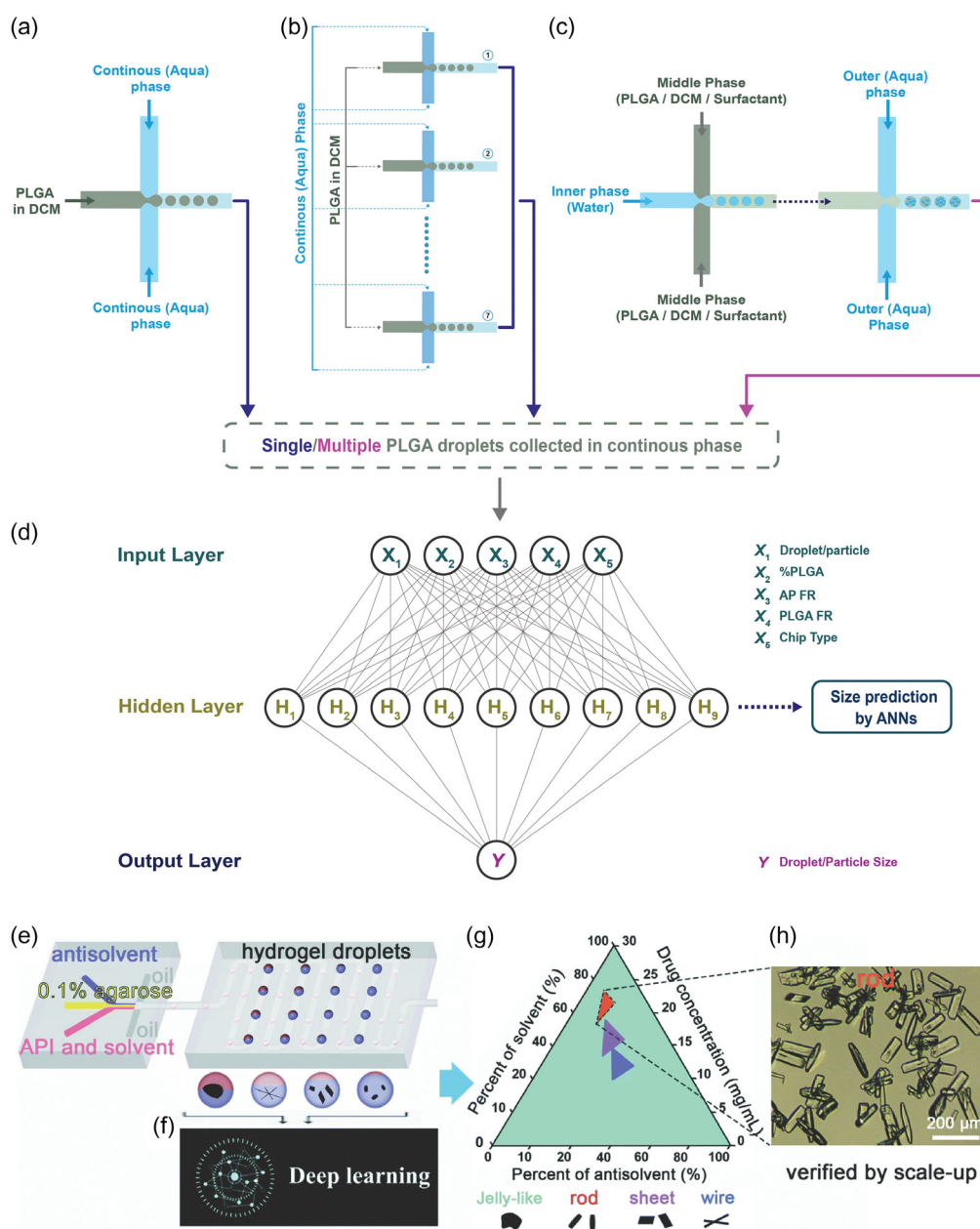


**Figure 6.** Synthesis of microparticles and morphology-controlled crystal growth and characterization. a) Schematic of the generation of monodisperse PLGA droplets using a single microfluidic device in single emulsion format, b) parallel generation using seven microfluidic devices, c) generation in multiple emulsion format, d) description of one of the ANN models employed to predict particle and droplet size from experimental data. AP: aqueous phase, FR: flow rate. (a–d) Reproduced with permission.<sup>[123]</sup> Copyright 2020, Springer Nature. e) Generation of hydrogel droplets with controlled ratio of solvent and anti-solvent, f) classification of the drug crystal morphologies by a deep learning algorithm, g) ternary phase diagram of the crystallization conditions and the obtained crystal morphologies depending on the API concentration and the ratio of solvent and antisolvent, and h) API rod crystals collected from a scale-up preparation according to the conditions identified in the ternary phase diagram. (e–h) Reproduced with permission.<sup>[124]</sup> Copyright 2020, The Royal Society of Chemistry.

A prominent example of this synergy is in flow cytometry, the gold standard technique in hematological diagnostics due to its ability to analyze large populations of cells and detect multiple molecular markers simultaneously. Traditional flow cytometry, however, lacks spatial resolution, as it only captures the intensity of cellular labels without spatial distribution information. Imaging flow cytometry (IFC) addresses this limitation by integrating the high throughput nature of flow cytometry with the spatial resolution of optical microscopy.<sup>[143,144]</sup> This circumvents, for example,

the challenges involved in defining molecular diagnostic markers and enhances morphology-based diagnosis of blood diseases through an automated procedure.<sup>[145]</sup> Machine learning algorithms, particularly CNNs, have significantly enhanced the analysis and interpretation of IFC data. Unlike classical image analysis methods that extract predefined features, CNNs learn to identify complex phenotypes by integrating multiple morphological and intensity features directly from image data, often detecting patterns invisible to the human eye.<sup>[146,147]</sup> By combining features

such as object area, object perimeter, pixel intensity, object shape, and granularity, CNNs can recognize more complex phenotypes based on specific combinations of morphological traits. Recent advancements in computer vision approaches have enabled the automated annotation of cell types from single-cell images acquired in IFC experiments.<sup>[148]</sup> Increasingly, these approaches have led to the development of “intelligent” image-based sorting systems. For instance, weakly supervised deep learning models such as iCellCnn have been used to diagnose diseases such as Sézary syndrome (a type of cutaneous T-cell lymphoma) with high accuracy, outperforming strongly supervised models,<sup>[149]</sup> and also demonstrating the potential to track disease progression for advanced-stage patients.

A key challenge in intelligent image-based cell sorting is balancing the large size and complexity of image data with processing speed, which directly impacts throughput. Recent advances have led to the development of two notable systems capable of high-speed, single-cell sorting based on imaging characteristics. One system utilizes a real-time image-guided sorting using spatial-temporal transformation and ML for classification,<sup>[134]</sup> while the other employs a deep CNN-assisted microfluidic sorting platform that operates at a throughput of approximately 2000 events per second.<sup>[4]</sup> The latter integrates high-throughput sorting with frequency-division, multiplexed microscopy and operates on a high-speed 10-Gbps architecture enabling the real-time capture and classification of fluorescence-labeled images, as exemplified in the sorting of microalgal and blood cells. These technologies represent significant milestones, as they enable sorting based on imaging features rather than just fluorescence intensity, linking cell phenotype to genotype and advancing both biological research and medical diagnostics.

Within droplet-based microfluidics, the integration of image-based single-cell sorting is especially promising for applications requiring both cell enrichment and single-cell encapsulation.<sup>[150]</sup> Importantly, ML-based image recognition can expand the breadth of sorting criteria beyond the simple distinction such as “empty” versus “cell-containing” droplets, to include morphological and functional traits. In this regard, Sesen et al. introduced an ML-enhanced image-based droplet sorting platform that classifies encapsulated single cells by morphology and selectively sorts those with desired traits. Unfortunately, the platform’s throughput was limited to 4 Hz,<sup>[133]</sup> a constraint that can be addressed by employing advanced CNNs integrated with optomechanical imaging methods.<sup>[151]</sup> In another study, Anagnostidis and coworkers improved the throughput to 40 Hz using deep neural networks for real-time droplet classification and sorting (**Figure 7a–d**)<sup>[101]</sup> and later adopted a deep learning object detector called YOLOv4-tiny (YOLO, for you only look once) to simultaneously identify single cells, single beads, and cell aggregates within droplets, achieving a throughput of up to 111 Hz in real time.<sup>[152]</sup> Using a closed feedback loop, they were able to control the loading of polyacrylamide beads inside droplets and finally demonstrated the combinatorial sorting of droplets coencapsulating both a single-cell and a single-bead. While imaging-based droplet sorting currently offers significantly lower throughput than traditional FACS (fluorescence activated cell sorting), it provides unique advantages, such as the ability to sort based on

morphological features and capturing spatially resolved data that is typically lost in single-point intensity measurements.

Beyond high-throughput classification and sorting, ML is being increasingly applied to the in-depth analysis of droplet contents, especially in single-cell assays and studies of cell–cell interactions. Soldati et al. demonstrated a CNN-based framework to classify droplet images as “empty,” “single-cell,” or “debris,” estimating extracellular acidification by measuring droplet and cell volumes, and predicting CD45 expression in white blood cells.<sup>[153]</sup> Similarly, Sarkar et al. developed an ML-based readout for a microfluidic droplet array to the interactions between natural killer (NK) cells and cancer cells—a key parameter for optimizing immunotherapeutic efficacy (**Figure 7e–g**).<sup>[154]</sup> Their approach leveraged single-cell formats to capture the heterogeneous nature of lymphocyte-target cell interactions. However, given the vast and complex datasets generated by high-throughput time-lapse imaging, they designed a DL model to analyze NK-target cell interactions within picoliter droplets. Their approach involved tracking conjugation duration between NK cells and targets, their interaction frequency, and cell death, using calcein AM fluorescence loss as a death marker. Following preprocessing, a CNN was trained to detect immune cell-target cell interactions and classify target cells as alive or dead. This integration of droplet microfluidics and ML thus enables precise, scalable analysis of immune activity against diverse cancer cell types.

ML has also significantly advanced the capabilities of organ-on-a-chip (OoC) technology, pushing the field beyond the limitations of traditional *in vitro* models. These models, particularly 2D monolayers, fail to replicate the complexity of *in vivo* microenvironments, where extracellular matrix interactions regulate cellular functions. While 3D cultures better preserve native cell behavior, they lack standardization and precise control over physiological stimuli.<sup>[155]</sup> OoC platforms overcome these limitations by leveraging microfluidic technology to provide a biomimetic microenvironment that enables systematic investigation of organ-specific functions under dynamic conditions, including responses to shear stress, mechanical forces, and biochemical gradients.<sup>[6,139]</sup> ML tools further enhance OoC platforms by automating device operation and improving the analysis of complex, high-content imaging data such as segmentation, classification, and feature detection.<sup>[156]</sup> Synergistic applications of ML in OoC platforms include automated evaluation of drug response,<sup>[140]</sup> real-time cell tracking,<sup>[132]</sup> extraction of quantitative biomarkers from live-cell imaging,<sup>[157]</sup> and predicting modeling of cellular responses to external stimuli.<sup>[158]</sup>

A powerful application of OoC models lies in their ability to simulate the mechanical and dynamic responses of organ-specific cells to uncover pathological dysfunctions, particularly in mechanically active tissues such as the lung and heart. Seminal work by Huh et al. demonstrated the utility of lung-on-chip systems in modeling pulmonary injury via liquid-plug dynamics<sup>[159]</sup> and assessing alveolar cell responses to nanoparticle exposure,<sup>[142]</sup> establishing these platforms as cost-effective alternatives for pre-clinical drug screening. Vascularized microphysiological systems (vMPS) represent another significant advancement. These systems closely mimic the structure and function of organ-specific tissues, making them highly valuable for drug screening and predicting patient-specific therapeutic outcomes.<sup>[160,161]</sup> In this context,

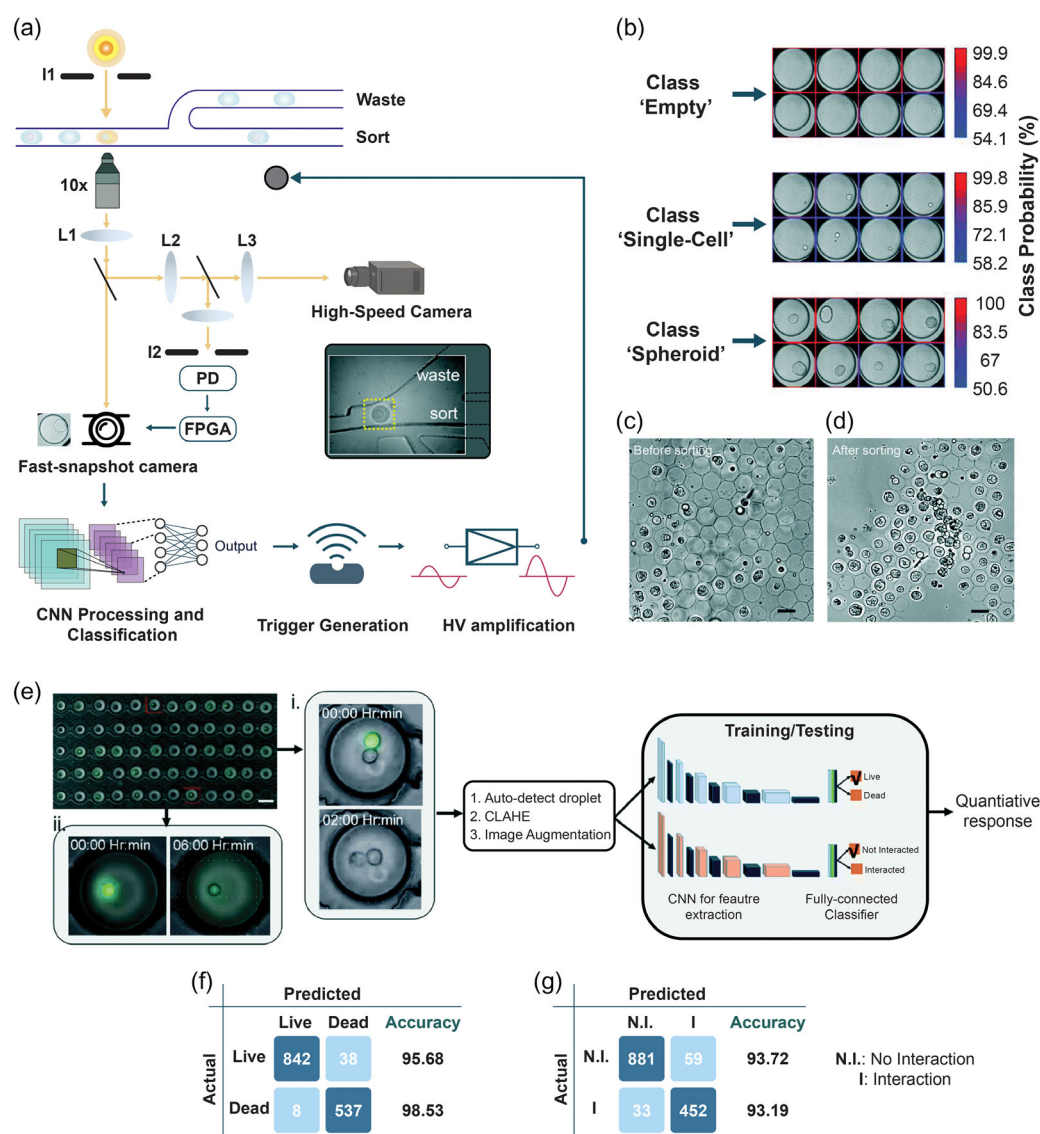


**Figure 7.** Image-based single-cell sorting. a) Illustration of the optical set-up for high-speed imaging and sorting of the droplets. b) Validation of the CNN for classification of three categories: empty droplet, droplet containing a single cell and droplet containing a spheroid. c) Collection of droplets before and d) after sorting. (a–d) Reproduced with permission.<sup>[101]</sup> Copyright 2020, The Royal Society of Chemistry. e) Overview of the microfluidic platform for the study of the cytotoxic effect of natural killer (NK) cells towards cancerous cells: time lapse microscopy of the droplets array containing cell pairs, followed by data processing via machine learning to identify cell–cell interactions and cell death. f) Confusion matrix for the prediction of live versus dead cells. g) Confusion matrix for the prediction of interaction versus noninteraction of cell pairs. (e–g) Reproduced with permission.<sup>[154]</sup> Copyright 2020, The Royal Society of Chemistry.

Tronolone et al. developed a microfluidic platform that enabled the self-assembly of perfusable vascular networks within a hydrogel matrix, effectively mimicking the *in vivo* capillary beds.<sup>[162]</sup> Due to the high computational cost of analyzing high-dimensional morphological data with the *in silico* developed AngioMT software, the authors employed ML models to predict oxygen transport efficiency from high-dimensional morphological data of vascular networks, outperforming traditional methods (Figure 8a–f). This approach accelerates the interpretation of complex datasets, facilitating the development of more reliable and biologically relevant OoC platforms.

Advanced microscopy combined with ML-driven analysis has also enabled real-time tracking of complex cell behaviors. For instance, Parlato et al. employed unsupervised learning to quantify

dendritic cell migration in tumor microenvironments, demonstrating how ML can extract subtle patterns from high-content imaging data.<sup>[163]</sup> Building upon this, Mencattini et al. introduced a deep learning-based framework called “Deep Tracking” which transforms single-cell motility trajectories, collected from time-lapse imaging of OoC platforms, into visual atlases (collection of images) analyzed by a pretrained CNN model, AlexNet (Figure 8g–i).<sup>[132]</sup> Applying this method to two biological scenarios, immune cell motility in vicinity of breast cancer cells and movement of prostate cancer cells, they achieved classification accuracy of 91.5% and 92% respectively for distinguishing drug-treated versus untreated conditions. Their study shows that deep learning can robustly decode complex motility patterns, providing a scalable and automated strategy for functional evaluation in OoC systems. While

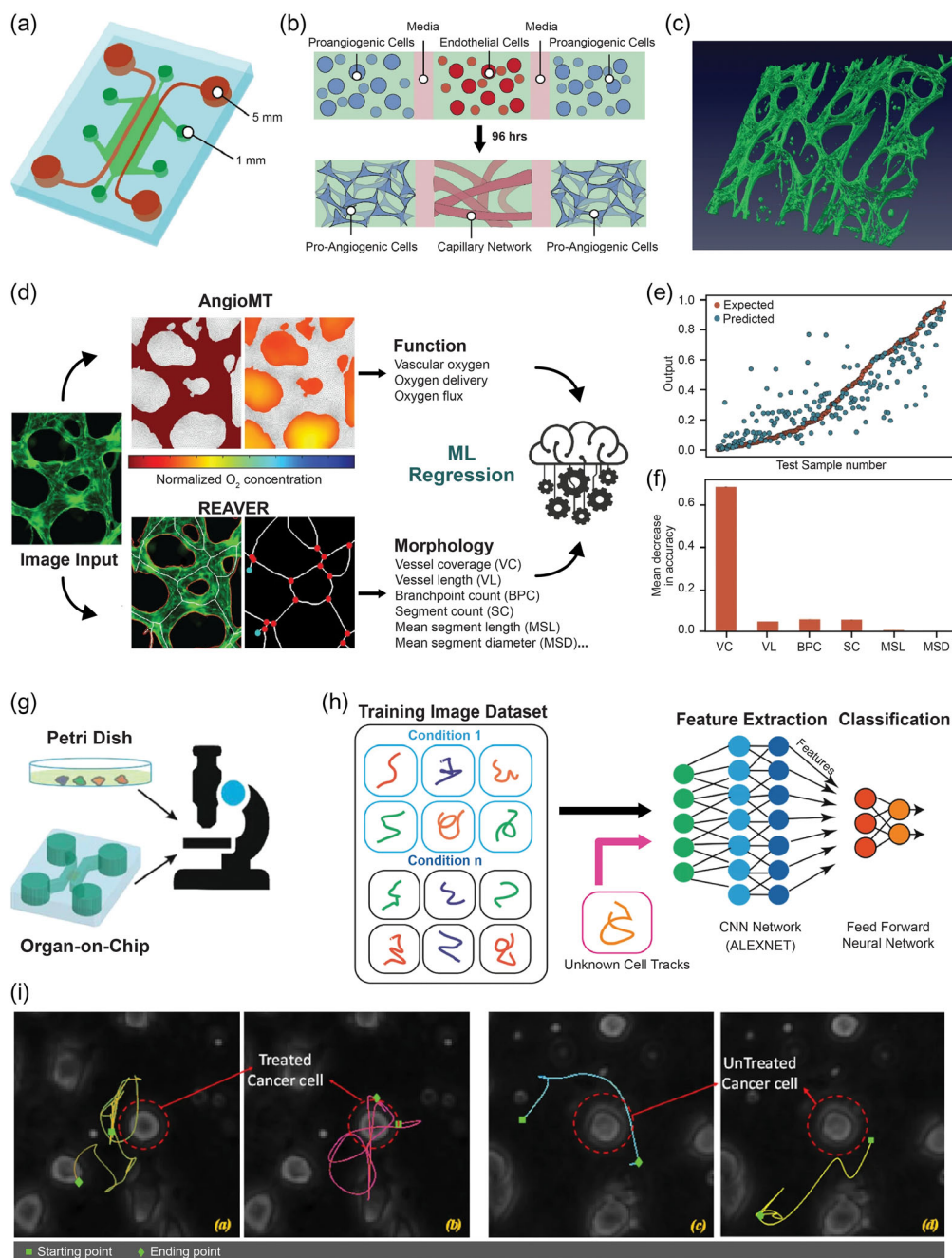


**Figure 8.** Organ-on-a-chip. a) Microfluidic device for compartmentalizing hydrogel (1 mm) and fluid (5 mm) in alternating channels to generate vascularized networks. b) Cell suspensions encapsulated in hydrogels and injected into the vascularized network. c) 3D reconstruction of formed vMPS. d) Functional and morphological metrics quantified by AngioMT and REAVR respectively are used to train the ML model to correlate both metrics and predict oxygen transport efficiency. e) Expected versus predicted results for the Random Forest regression model. f) comparing inputs to determine the strongest contributor to model. (a–f) Reproduced with permission.<sup>[162]</sup> Copyright 2023, Springer. g) Time-lapse imaging used to record video sequence of moving cells and tracking cell trajectories with the Cell Hunter tool. h) Atlases of cell trajectories collected for different biological conditions are used to train a deep learning architecture to extract features and classify cell motility behavior. i) Case study to investigate trajectories of immune cells in proximity of a treated (with drug trastuzumab) and untreated cancer cell over a period of 72 h. (g–i) Reproduced with permission.<sup>[132]</sup> Copyright 2020, Springer Nature.

real-time control and monitoring in mechanically active OoC platforms are still in their early stages, deep learning is already enhancing feature extraction, image analysis, and data interpretation. As OoC models continue to evolve, the integration of ML will be central to scaling up toward multiorgan “human-on-a-chip” platforms, ultimately advancing personalized medicine and accelerating drug development.<sup>[164,165]</sup>

### 4.3. Microfluidic System Design

The effectiveness of CMFs in chemistry and biology fundamentally depends on optimal device design, which requires the ability to accurately predict flow dynamics and fluid patterns for specific applications. While laminar flows typically used in microfluidics provide precise fluidic control, the overall design, fabrication,

and operation of devices remains complex, particularly for non-linear, multiphase flows (such as droplet-based systems) or setups integrating active components like valves, pumps, and mixers.<sup>[166]</sup> These complexities, combined with the inherently multi-modal nature of the design space where multiple geometric configurations can yield similar flow profiles, make empirical trial-and-error approaches impractical for large-scale adoption. To overcome these challenges, automated and intelligent design with ML models, such as deep learning algorithms and neural networks, can help constrain the design space and predict configurations that meet specific flow requirements.<sup>[68,167]</sup>

ML-driven optimization not only accelerates the iterative “design-test-modify” cycle but also improves convergence on optimal architectures for both continuous and segmented flow. A prime example is the use of ML in flow sculpting, where specific micropillar arrangements within a microchannel dictate the outlet fluid shape.<sup>[168]</sup> Each pillar induces a localized deformation, and the cumulative effect of the sequence creates complex, user-defined cross-sectional flow profiles. By mapping these relationships, a library of known sequence-flow patterns can be generated. This then serves as training data for ML algorithms to predict sculpted flow shapes for a given pillar configuration. Stockstein and coworkers pioneered this concept by combining flow sculpting with a genetic algorithm-guided approach.<sup>[169]</sup> Using a custom lightweight software package called uflow, they transitioned from simple sequences (1–3 pillars) to more complex architectures. They optimized eight microfluidic workflows, including splitting, encapsulation, and stretching, and demonstrated strong agreement between simulations and fabricated devices. The study highlighted the use of this strategy in several applications, such as 3D-shaped particle formation,<sup>[170]</sup> fabrication of polymeric fibers,<sup>[171]</sup> and controlling cell/particle behavior in a fluid streams.<sup>[172]</sup> Despite its success, genetic algorithm-based optimization suffers from stochastic variability and long computation times. To address these limitations, recent studies have introduced a deep learning framework incorporating intelligent sampling and dimensionality reduction, enabling efficient exploration of vast combinatorial design spaces ( $\approx 32$  billion pillar sequences) and accurate prediction of optimal configurations for complex flow shapes (Figure 9).<sup>[173]</sup> The potential of this approach goes beyond flow sculpting in tackling other complex inverse design problems across different scientific domains.<sup>[174]</sup>

Microfluidic systems often require the user to define the initial conditions (e.g., reagent concentrations or inlet/outlet pressure) and flow parameters to maintain stable operation, largely due to device-to-device variations from fabrication and unforeseen disturbances such as channel fouling or noise in sensor signals. These factors can disrupt flow and necessitate manual intervention, limiting the consistency and autonomy of long-term experiments. To address such situations, Dressler et al. implemented two different RL algorithms, based on neural networks (Deep Q-Network)<sup>[175]</sup> and episodic memory (Model-Free Episodic Controller (MFEC) algorithm),<sup>[176]</sup> to autonomously control microfluidic flows.<sup>[103]</sup> These RL agents were trained to solve two tasks: interface positioning in continuous laminar flow and droplet size modulation in segmented flow. Through reward-based feedback from real-time bright-field images, both RL agents outperformed

trained human operators in maintaining optimal flow conditions. Notably, the MFEC model achieved rapid convergence for droplet size control, requiring only a few minutes of training, highlighting RL’s potential to enhance autonomy and reliability in microfluidic experimentation.

Targeted generation and classification of droplets is a complex phenomenon dependent upon channel geometry and interfacial flow dynamics, making the task well-suited for ML-guided optimization. For instance, droplet stability is crucial in segmented-flow biochemical assays, where maintaining an isolated and controlled environment is essential for accurate and reliable results. To address this, Khor et al. applied a convolutional autoencoder model to analyze local stresses experienced by droplets within concentrated emulsions, using bright-field images to identify an 8-dimensional shape descriptor able to capture diverse droplet morphologies.<sup>[177]</sup> This descriptor was able to predict droplet breakup when passing through constrictions, revealing key influencing factors such as droplet generation conditions, throat size, and surface curvature.

Considering advanced ML algorithms, deep learning is one approach that excels at extracting features from images, making it particularly effective for tracking droplets and their encapsulated particles. In this context, Durve et al. developed a deep learning tool trained on synthetic datasets that tracks droplet trajectories at 400 frames per second, demonstrating strong generalization to real experimental data.<sup>[178]</sup> Similarly, Hadikhani et al. developed a DNN-enabled droplet microfluidic platform to estimate fluidic parameters such as flow rate and component concentration from optical images of water–alcohol droplets.<sup>[179]</sup> Their workflow predicted dynamic flow changes and regime transitions in real time without the integration of bulky sensors, ultimately simplifying microfluidic chip design and fabrication.

ML has also been applied to evaluate and sort dynamic behaviors within droplets. In one study, DNNs were trained to detect and quantify mixing in merged droplet pairs, classifying them into low, intermediate, or high mixing categories. The authors deployed two CNN architectures, a lightweight real-time object detection network from the YOLO series<sup>[180]</sup> and a Singleshot Multibox Detector (SSD),<sup>[181]</sup> to analyze large image datasets and evaluate mixing patterns, providing insights into droplet coalescence based on distinct features. ML-integrated optical monitoring can also be used to improve performance metrics in microfluidic platforms, as demonstrated through the real-time classification and sorting of microcapsules. For instance, Chu et al. designed an automated classification and sorting system for double emulsion droplets using CNN analysis of real-time images.<sup>[182]</sup> By identifying droplets in the desirable dripping state, the system triggered a valve-based sorter to collect monodisperse microcapsules during active production. Such integration of ML for real-time classification and actuation underscores the growing capabilities of CMFs as autonomous analytical and synthetic tools. These advances collectively demonstrate that reinforcement learning and other ML techniques can significantly reduce the need for manual intervention in microfluidic experiments, enabling continuous, adaptive, and high-precision operation even in the face of unpredictable disturbances.

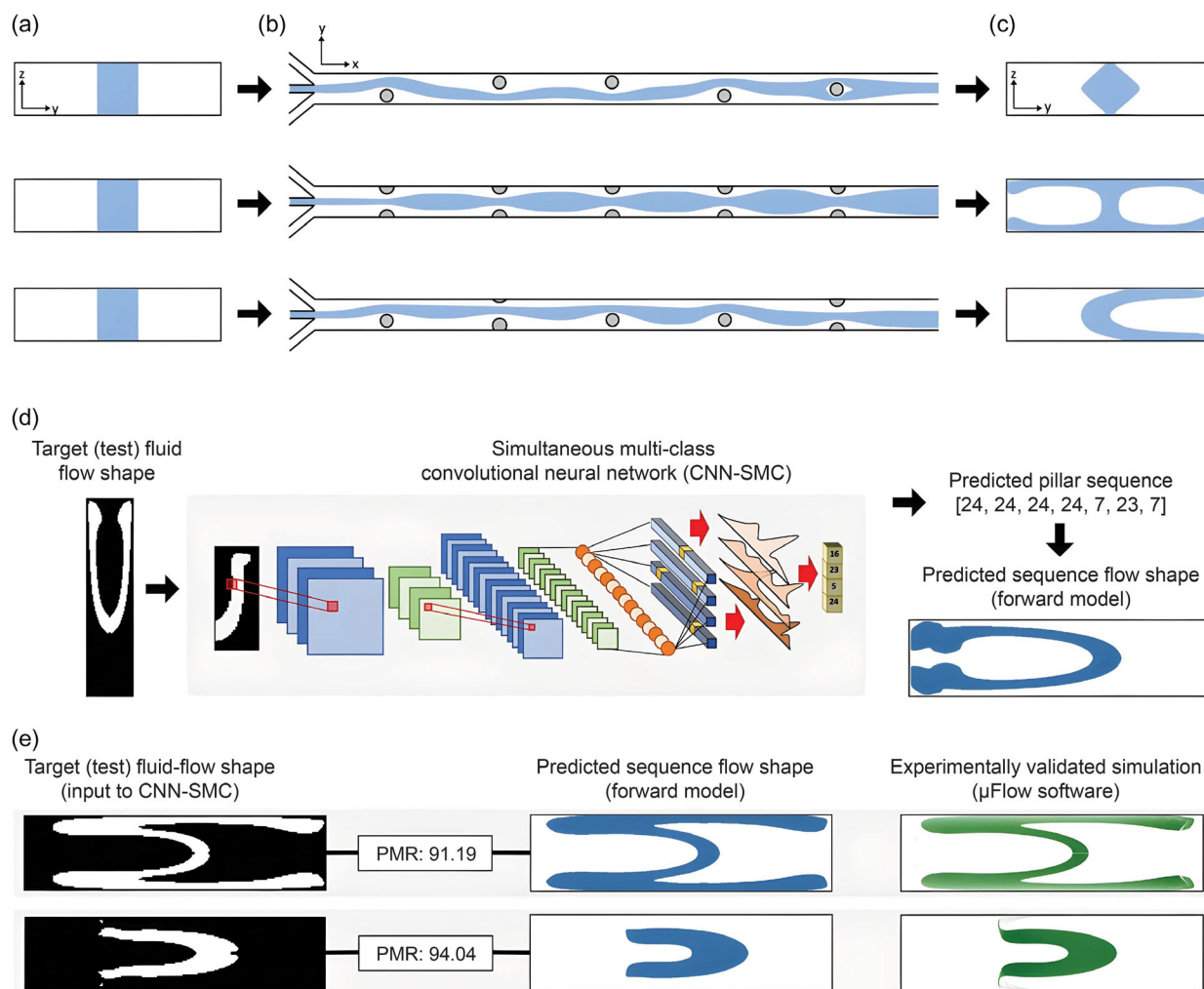


**Figure 9.** Flow sculpting. a) Same inlet flow configuration (cross-sectional view of the channel containing fluid, in blue) passing through, b) three different micropillar sequences (top-down view) each inducing a different localized deformation to the fluid, resulting in, c) user-defined cross-section profiles at the outlet, and d) target fluid flow shapes fed as input to the CNN model predicting the pillar sequence as an output. This output is further used as input to the forward model to create the predicted sequence flow shape, as exemplified for e) two different target inputs. Reproduced with permission.<sup>[173]</sup> Copyright 2017, Springer Nature.

Beyond image-based classification and control, machine learning and algorithmic frameworks have been increasingly applied to the a priori design of microfluidic devices. A key example is DAFD (Design Automation of Fluid Dynamics), a web-based design tool developed by Lashkaripour and coworkers that automates the design and performance prediction of flow-focusing droplet generators (Figure 10).<sup>[60]</sup> DAFD leverages neural network models trained on extensive experimental datasets, including 888 data points from 43 devices spanning different dripping and jetting regimes, to accurately predict droplet diameter and generation rate with mean absolute percentage errors (MAPE) below 4.2% and 11.5%, respectively. Importantly, DAFD maintains high predictive fidelity even for previously unseen flow conditions and achieves 100% accuracy in classifying droplet generation regimes, significantly reducing the need for iterative design and specialized microfluidic expertise.

Finally, it is also important to mention advancements in computer-aided design (CAD) of microfluidic devices that facilitate the transition from conceptual microfluidic designs to

actual devices by integrating description languages and optimization algorithms. As operations grow more complex, such as in fully programmable valve arrays (FPVAs),<sup>[183]</sup> the density of valves controlling fluidic manipulations increases at rates surpassing Moore's law.<sup>[184]</sup> CAD tools systematically incorporate design heuristics, physical constraints, and numerical models to automate design and reduce manual effort for complex architectures. For instance, Amin and coworkers introduced the microfluidic instruction set architecture (ISA), a hardware description language that allows designers to specify fluidic operations logically, such as parallel or sequential flows, which are then translated into optimized device layouts.<sup>[185]</sup> Tools such as Fluigi<sup>[186]</sup> facilitate the optimization of multilevel genetic circuits, while Columba<sup>[187]</sup> allows co-optimization of flow and control layers in multilayered devices. Additionally, platforms such as 3DμF<sup>[188]</sup> offer integrated libraries of parameterized components and support standardized interchange formats, enhancing design sharing and reproducibility. Collectively, these advancements in ML-driven prediction and CAD-based

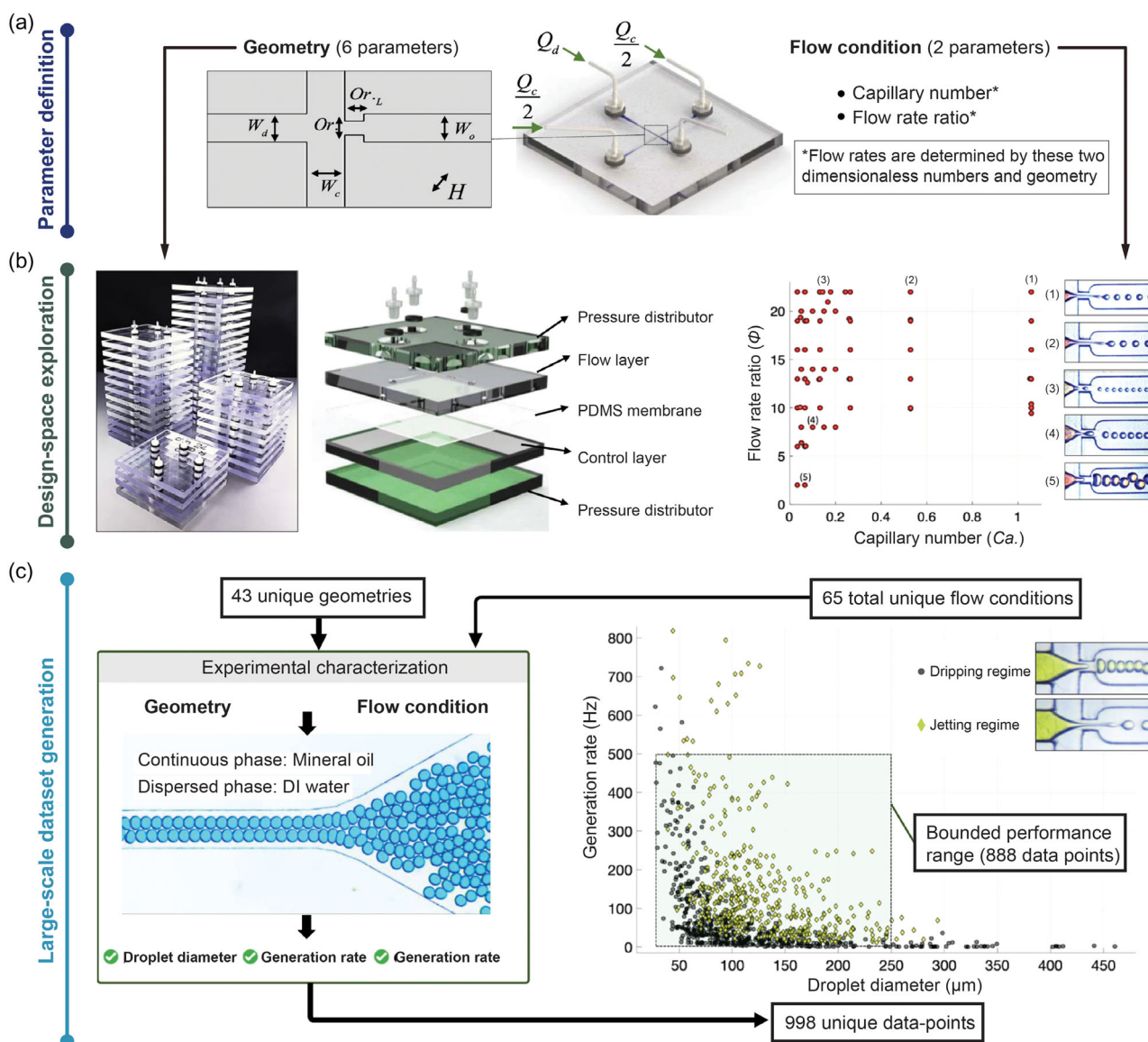


**Figure 10.** Design of flow-focusing droplet generators. a) A set of flow-focusing geometries with different parameters was identified following an orthogonal design of experiments. For each device, the flow rates to test were identified from the capillary number and flow rate ratio. b) Rapid prototyping of 43 devices using a micromill and a layer assembly. The operation of each device over a wide range of conditions generates a large-scale dataset. c) For every condition, the droplets were imaged and the droplet diameter, generation frequency, and generation regime (dripping, jetting) were recorded. Reproduced with permission.<sup>[60]</sup> Copyright 2021, Springer Nature.

automation are transforming the microfluidic design landscape, reducing number of steps in the design cycle, improving reproducibility, and enhancing functionality, testability and scalability in microfluidic operations across diverse domains.

## 5. Challenges and Perspective

The integration of combinatorial microfluidics with machine learning holds transformative potential for chemistry and biology, enabling precise, automated manipulation of fluids and obtaining data-driven insights from complex, multi-dimensional experiments. However, realizing the full promise of this synergy is far from straightforward and faces several significant

challenges related to hardware scalability, design standardization, data quality, black-box optimization, and interoperability (Figure 11).

One of the biggest hurdles from a hardware perspective is the complexity and scalability of the external control systems required to operate dense and large-scale valve systems. These multiplexed architectures often demand individual control lines for each valve or pump, leading to cumbersome and intricate setups that are difficult to scale for high-throughput applications. While emerging solutions, such as serial instruction schemes (e.g., frequency-based or latching valves) and embedded systems (e.g., self-regulating fluidic circuits) can reduce the number of external connections required, these approaches are likely to compromise operational flexibility.<sup>[189]</sup>

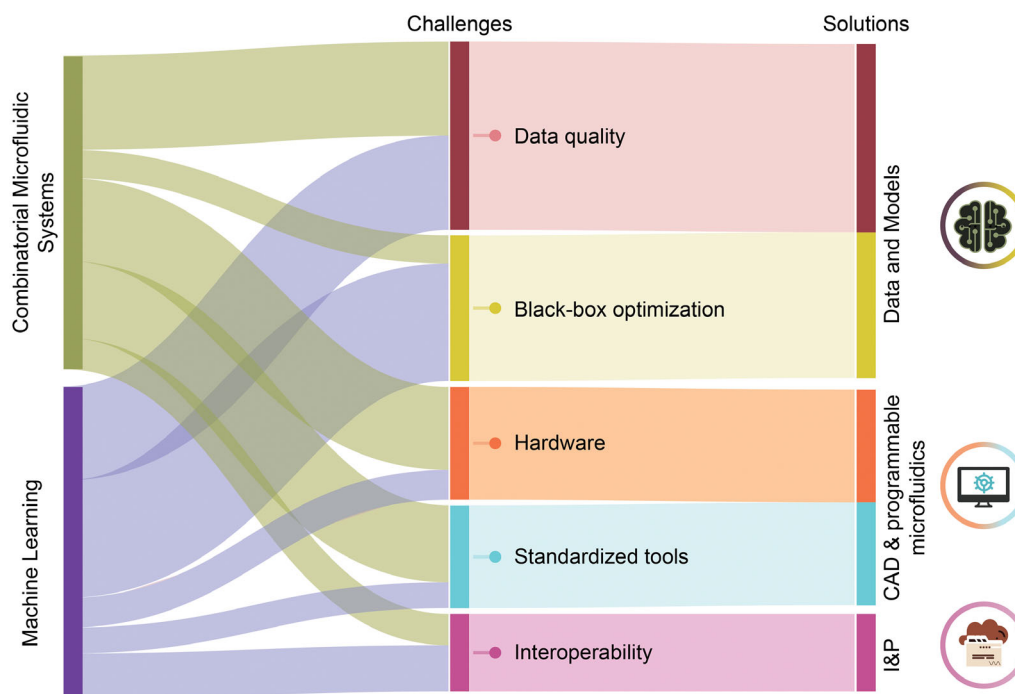


**Figure 11.** Challenges and solutions. Schematic representation of key challenges at the interface of combinatorial microfluidic systems and machine learning and potential solution domains. The diagram maps major obstacles—such as data quality, black-box optimization, hardware limitations, lack of standardized tools, and interoperability—arising from CMFs, ML, or both, to three solution domains: data and models, fluidic CAD tools and programmable microfluidics, and infrastructure and protocols (I&P). The thickness of connecting lines reflects a qualitative assessment of each field's relative contribution to a given challenge based on literature survey (Web of Science), emphasizing conceptual weight rather than quantitative metrics.

Another promising approach is using digital microfluidic (DMF)-based devices, which use electrowetting to manipulate droplets on a 2D electrode array. This replaces the use of microvalves and micropumps as is the case in first generation microfluidic biochips. DMF offers programmability akin to electronics, enabling dynamic reconfiguration of fluidic pathways. However, persistent issues such as droplet evaporation, cross-contamination, and electrode degradation remain barriers to its widespread adoption and underscore the need for a more robust framework for programmable fluidic design. This pursuit is currently constrained by the lack of mature, dedicated CAD tools tailored to the unique requirements of microfluidic device design. Unlike electronics, where tools like SPICE<sup>[190]</sup> can abstract transistor behavior into predictable models for modular circuit design, microfluidics lacks an equivalent “circuit designer’s toolkit”. As a result, most complex microfluidic systems are still assembled through a bottom-up approach, requiring significant manual effort to engineer, test, and integrate individual modules (e.g., mixers, valves, or storage reservoirs) into a complete, functional system.<sup>[191]</sup> This process is exhausting and becomes a bottleneck as designs scale up and the need for rapid prototyping and deployment increases.

While early efforts such as BioStream,<sup>[192]</sup> a programming language for fluidic operations, and AquaCore,<sup>[193]</sup> a microfluidic instruction set architecture inspired by MEMS design, represent promising steps toward designing programmable microfluidic operations, these platforms are still in their infancy and lack the seamless modular integration found in electronic CAD

environments. The field still awaits standardized “Lego block” libraries and high-level abstraction layers that would allow designers to rapidly assemble and optimize multicomponent microfluidic systems. Widespread development and adoption of precharacterized modules for mixing, droplet generation, and storage could significantly streamline the design process, much like standardized logic gates transformed electronic circuit design.

The machine learning side of integrated ML-microfluidic systems faces several significant and nontrivial challenges, primarily related to scalability, data quality, and generalizability. Traditional ML models in science are primarily performance-oriented, using relatively structured (labeled) and limited datasets for tasks like classification or regression.<sup>[57]</sup> However, as microfluidic applications scale, as in materials discovery or molecular design, the computational burden rises steeply. Deep neural networks excel at modeling complex relationships, but as their architectures grow deeper (more hidden layers) and more parameter-rich, they demand significant training time and energy. For example, the continuously expanding GDB database, developed to assist de novo drug design,<sup>[194]</sup> contains 166 billion synthetically accessible drug-like molecule; training a model on the GDB-17 database is computationally prohibitive for most research labs, even with access to supercomputers.<sup>[195]</sup> However, such computational infrastructure is neither widely available or cost-effective for most research environments, especially when scaling further to chemical species with 40–50 atoms. This scalability bottleneck necessitates the adoption of ML strategies that reduce

computational demands, such as model compression techniques (e.g., knowledge distillation),<sup>[196]</sup> efficient architectures like graph neural networks (GNNs),<sup>[197]</sup> and transfer learning approaches that repurpose pretrained models for new tasks with lower computational cost and minimal loss in performance.<sup>[198]</sup>

Beyond scalability, data quality remains a fundamental concern. ML models are highly sensitive to the quality and consistency of training data. In microfluidic platforms, data is often sourced from high-throughput imaging or sensor measurements, which may be noisy, redundant, or poorly annotated. In addition, variability in experimental protocols such as flow rates, shear conditions, and sensor calibration can introduce systematic biases that render models ineffective when applied to data from different instruments or labs.<sup>[62]</sup> For instance, manual annotation of >100,000 single-cell images per experiment in IFC remains prohibitively labor-intensive, despite recent advances in automated labeling algorithms.<sup>[149]</sup> Weakly supervised approaches, such as iCellCnn, have been used to reduce this burden by using specimen-level labels instead of single-cell annotations. The high-dimensionality and nonlinearity of cytometry data further complicate model performance. Conventional models such as logistic regression struggle with these challenges, while neural networks, though powerful for image analysis, are limited from the lack of interpretability. This “black-box” nature becomes especially concerning in settings like drug discovery or clinical diagnostics, where understanding how a model arrives at its predictions is essential for trust and adoption.<sup>[199]</sup>

Translating automated microfluidic innovations into commercial settings introduces additional complexity. Early successes, such as the Agilent 2100 Bioanalyzer for DNA and protein electrophoresis,<sup>[200,201]</sup> Bio-Rad’s Droplet Digital PCR (ddPCR) system for precise nucleic acid quantification,<sup>[202]</sup> and NuGEN’s Mondrian digital microfluidics system for automating library preparation,<sup>[203]</sup> demonstrate how integrating microfluidics with automation can reshape laboratory workflows. However, most academic automation platforms remain bespoke, with custom hardware-software integrations that resist scalability or reuse. To advance, the next generation of lab-on-chip platforms must accommodate a wide-range of assays, support ML-driven optimization, and work reliably across different instruments, users, and environments. Just as important is the underlying informatics infrastructure, ontologies, metadata standards, and transparent protocol management, which is essential for reproducibility at scale.<sup>[201]</sup> Without this, even the most elegant automation can fall short in commercial settings.

Addressing these challenges demands a comprehensive, interdisciplinary framework. Communication standards such as SiLA 2 (Standardization in Laboratory Automation) can help simplify instrument integration by providing a common operational language, eliminating the need for custom drivers or software.<sup>[204]</sup> When combined with open data standards such as AnIML (Analytical Information Markup Language), this enables true interoperability, machine readability, and reproducibility; features that are essential for real-time ML integration and cloud-driven experimental control.<sup>[205,206]</sup> Together, SiLA and AnIML can underpin the development of flexible, modular, and auditable automation infrastructures. Global biofoundries<sup>[204]</sup> and centralized

cloud-based infrastructures (like Emerald Cloud Lab or Strateos)<sup>[207]</sup> are already leveraging these principles to streamline high-throughput experimentation through centralized control, standardized protocols, and accessible automation. These frameworks lower the barrier for deploying ML-integrated microfluidic workflows at scale.

Looking forward, generative AI tools, such as diffusion models, can create synthetic cell images or simulate microfluidic flow fields to fill gaps in datasets and improve model performance. Furthermore, using explainable AI (XAI) (e.g., attention maps and saliency methods) can allow the researcher to know what operations go on behind the scene, increasing accuracy in the detection of false positives in clinical applications.<sup>[208,209]</sup> Ultimately, widespread adoption and commercialization of ML-integrated microfluidics will depend on balancing flexibility with standardization, fostering collaboration among engineers, biologists, and data scientists, and establishing rigorous validation protocols that include testing with end-users in real-world settings.<sup>[210]</sup>

## 6. Concluding Remarks

The synergy between CMFs and ML offers significant promise across various fields, including material synthesis, reaction optimization, biological assays, and enhanced microfluidic device design. By leveraging the strengths of both technologies, precise fluid manipulation and high-throughput experimentation with CMFs and powerful data analysis and prediction using ML, researchers are creating intelligent, automated systems capable of real-time optimization, high-throughput screening, and adaptive experimental workflows. Despite this promise, several challenges remain. Hardware scalability, the need for consistent and high-quality data, and the lack of standardized design tools continue to limit widespread adoption. Like an orchestra where every instrument must be in sync, integrating CMFs and ML requires thoughtful coordination across hardware, software, experimental design, and data infrastructure. This is especially critical as applications grow in complexity and move toward commercial and clinical settings, where reliability and regulatory compliance become paramount. Progress is being made through interdisciplinary collaboration, development of robust data pipelines, federated learning frameworks, and community-driven design tools. By addressing current limitations head on, the community can unlock the full potential of the CMFs-ML synergy, transforming healthcare, chemical research, and industrial processes for the future.

## Acknowledgements

The authors acknowledge Eidgenössische Technische Hochschule Zürich and NCCR Catalysis (grant no. 180544), a National Centre of Competence in Research funded by the Swiss National Science Foundation for financial support.

Open access publishing facilitated by Eidgenössische Technische Hochschule Zurich, as part of the Wiley - Eidgenössische Technische Hochschule Zurich agreement via the Consortium Of Swiss Academic Libraries.

## Conflict of Interest

The authors declare no conflict of interest.

**Keywords:** biology · chemistry · combinatorial microfluidics · machine learning · microfluidic system design

- [1] N. Convery, N. Gadegaard, *Micro Nano Eng.* **2019**, *2*, 76.
- [2] G. M. Whitesides, *Nature* **2006**, *442*, 368.
- [3] J. Liu, H. Du, L. Huang, W. Xie, K. Liu, X. Zhang, S. Chen, Y. Zhang, D. Li, H. Pan, *ACS Appl. Mater. Interfaces* **2024**, *16*, 38832.
- [4] N. Nitta, T. Sugimura, A. Isozaki, H. Mikami, K. Hiraki, S. Sakuma, T. Iino, F. Arai, T. Endo, Y. Fujiwaki, H. Fukuzawa, M. Hase, T. Hayakawa, K. Hiramatsu, Y. Hoshino, M. Inaba, T. Ito, H. Karakawa, Y. Kasai, K. Koizumi, S. Lee, C. Lei, M. Li, T. Maeno, S. Matsusaka, D. Murakami, A. Nakagawa, Y. Oguchi, M. Oikawa, et al., *Cell* **2018**, *175*, 266.
- [5] M. Alvarez, E. Rahmani, B. Jew, K. M. Garske, Z. Miao, J. N. Benhammou, C. J. Ye, J. R. Pisegna, K. H. Pietiläinen, E. Halperin, P. Pajukanta, *Sci. Rep.* **2020**, *10*, 11019.
- [6] S. N. Bhatia, D. E. Ingber, *Nat. Biotechnol.* **2014**, *32*, 760.
- [7] H. Li, A. J. Steckl, *Anal. Chem.* **2019**, *91*, 352.
- [8] L. Liu, M. Bi, Y. Wang, J. Liu, X. Jiang, Z. Xu, X. Zhang, *Nanoscale* **2021**, *13*, 19352.
- [9] J. P. McMullen, K. F. Jensen, *Annu. Rev. Anal. Chem.* **2010**, *3*, 19.
- [10] A. Abou-Hassan, O. Sandre, V. Cabuil, *Angew. Chem. Int. Ed.* **2010**, *49*, 6268.
- [11] Z. Zhou, X. Li, R. N. Zare, *ACS Cent. Sci.* **2017**, *3*, 1337.
- [12] I. E. Araci, P. Brisk, *Curr. Opin. Biotechnol.* **2014**, *25*, 60.
- [13] T. Thorsen, S. J. Maerkl, S. R. Quake, *Science* **2002**, *298*, 580.
- [14] C. Neils, Z. Tyree, B. Finlayson, A. Folch, *Lab. Chip* **2004**, *4*, 342.
- [15] Y. Zhang, T.-H. Wang, *RSC Adv.* **2019**, *9*, 21741.
- [16] B. R. Schudel, C. J. Choi, B. T. Cunningham, P. J. A. Kenis, *Lab. Chip* **2009**, *9*, 1676.
- [17] T. F. Didar, M. Tabrizian, *Lab. Chip* **2012**, *12*, 4363.
- [18] Y. Zhou, Y. Wang, T. Mukherjee, Q. Lin, *Lab. Chip* **2009**, *9*, 1439.
- [19] S. K. W. Dertinger, D. T. Chiu, N. L. Jeon, G. M. Whitesides, *Anal. Chem.* **2001**, *73*, 1240.
- [20] X. Wang, Z. Liu, Y. Pang, *RSC Adv.* **2017**, *7*, 29966.
- [21] R. Utharala, A. Grab, V. Vafaizadeh, N. Peschke, M. Ballinger, D. Turei, N. Tuechler, W. Ma, O. Ivanova, A. G. Ortiz, J. Saez-Rodriguez, C. A. Merten, *Nat. Protoc.* **2022**, *17*, 2920.
- [22] B. Schuster, M. Junkin, S. S. Kashaf, I. Romero-Calvo, K. Kirby, J. Matthews, C. R. Weber, A. Rzhetsky, K. P. White, S. Tay, *Nat. Commun.* **2020**, *11*, 5271.
- [23] Z. Zhang, Y.-C. Chen, S. Urs, L. Chen, D. M. Simeone, E. Yoon, *Small* **2018**, *14*, 1703617.
- [24] F. Eduati, R. Utharala, D. Madhavan, U. P. Neumann, T. Longerich, T. Cramer, J. Saez-Rodriguez, C. A. Merten, *Nat. Commun.* **2018**, *9*, 2434.
- [25] A. B. Theberge, E. Mayot, A. E. Harrak, F. Kleinschmidt, W. T. S. Huck, A. D. Griffiths, *Lab. Chip* **2012**, *12*, 1320.
- [26] W. Gu, X. Zhu, N. Futai, B. S. Cho, S. Takayama, *Proc. Natl. Acad. Sci.* **2004**, *101*, 15861.
- [27] B. Zhang, H. Xu, Y. Huang, W. Shu, H. Feng, J. Cai, J. F. Zhong, Y. Chen, *Analyst* **2019**, *144*, 7185.
- [28] S. J. Maerkl, S. R. Quake, *Science* **2007**, *315*, 233.
- [29] S. Keller, S. P. Teora, M. Boujemaa, D. A. Wilson, *Biomacromolecules* **2021**, *22*, 1759.
- [30] P. J. Resto, B. J. Mogen, E. Berthier, J. C. Williams, *Lab. Chip* **2010**, *10*, 23.
- [31] M. A. Unger, H. P. Chou, T. Thorsen, A. Scherer, S. R. Quake, *Science* **2000**, *288*, 113.
- [32] S. Derveaux, B. G. Stubbe, K. Braeckmans, C. Roelant, K. Sato, J. Demeester, S. C. De Smedt, *Anal. Bioanal. Chem.* **2008**, *391*, 2453.
- [33] C. Pöhlmann, T. Elßner, *Toxins* **2020**, *12*, 727.
- [34] D. A. Cusanovich, R. Daza, A. Adey, H. A. Pliner, L. Christiansen, K. L. Gunderson, F. J. Steemers, C. Trapnell, J. Shendure, *Science* **2015**, *348*, 910.
- [35] L. A. Bawazer, C. S. McNally, C. J. Empson, W. J. Marchant, T. P. Comyn, X. Niu, S. Cho, M. J. McPherson, B. P. Binks, A. deMello, F. C. Meldrum, *Sci. Adv.* **2016**, *2*, e1600567.
- [36] D. Berrar, *Data Min. Knowl. Discov.* **2022**, *36*, 1102.
- [37] J. K. Kruschke, *Trends Cogn. Sci.* **2010**, *14*, 293.
- [38] M. Lin, H. C. Lucas, G. Shmueli, *Inf. Syst. Res.* **2013**, *24*, 906.
- [39] A. Krogh, *Nat. Biotechnol.* **2008**, *26*, 195.
- [40] Y. Wu, J. Feng, *Wirel. Pers. Commun.* **2018**, *102*, 1645.
- [41] M. Pak, S. Kim, in *2017 4th Int. Conf. on Computer Applications and Information Processing Technology (CAIPT)*, Kuta Bali, Indonesia, IEEE, New York City, USA **2017**, pp. 1–3.
- [42] K. R. Chowdhary, in *Fundamentals of Artificial Intelligence* (Ed: K. R. Chowdhary), Springer, India, New Delhi **2020**, pp. 603–649.
- [43] J. Ma, R. P. Sheridan, A. Liaw, G. E. Dahl, V. Svetnik, *J. Chem. Inf. Model.* **2015**, *55*, 263.
- [44] M. H. S. Segler, M. Preuss, M. P. Waller, *Nature* **2018**, *555*, 604.
- [45] A. W. Senior, R. Evans, J. Jumper, J. Kirkpatrick, L. Sifre, T. Green, C. Qin, A. Židek, A. W. R. Nelson, A. Bridgland, H. Penedones, S. Petersen, K. Simonyan, S. Crossan, P. Kohli, D. T. Jones, D. Silver, K. Kavukcuoglu, D. Hassabis, *Proteins Struct. Funct. Bioinforma.* **2019**, *87*, 1141.
- [46] T.-H. Wang, C.-Y. Lee, T.-Y. Lee, H.-D. Huang, J. B.-K. Hsu, T.-H. Chang, *Cancers* **2021**, *13*, 2528.
- [47] E. A. Galan, H. Zhao, X. Wang, Q. Dai, W. T. S. Huck, S. Ma, *Matter* **2020**, *3*, 1893.
- [48] A. L'Heureux, K. Grolinger, H. F. Elyamany, M. A. M. Capretz, *IEEE Access* **2017**, *5*, 7776.
- [49] X. Huang, T.-Y. Ho, W. Guo, B. Li, K. Chakrabarty, U. Schlichtmann, *ACM Comput. Surv.* **2022**, *54*, 1.
- [50] J. Jumper, R. Evans, A. Pritzel, T. Green, M. Figurnov, O. Ronneberger, K. Tunyasuvunakool, R. Bates, A. Židek, A. Potapenko, A. Bridgland, C. Meyer, S. A. A. Kohli, A. J. Ballard, A. Cowie, B. Romera-Paredes, S. Nikolov, R. Jain, J. Adler, T. Back, S. Petersen, D. Reiman, E. Clancy, M. Zielinski, M. Steinegger, M. Pacholska, T. Berghammer, S. Bodenstein, D. Silver, et al., *Nature* **2021**, *596*, 583.
- [51] R. Nussinov, M. Zhang, Y. Liu, H. Jang, *J. Phys. Chem. B* **2022**, *126*, 6372.
- [52] M. Varadi, D. Bertoni, P. Magana, U. Paramval, I. Pidruchna, M. Radhakrishnan, M. Tsenkov, S. Nair, M. Mirdita, J. Yeo, O. Kovalevskiy, K. Tunyasuvunakool, A. Laydon, A. Židek, H. Tomlinson, D. Hariharan, J. Abrahamson, T. Green, J. Jumper, E. Birney, M. Steinegger, D. Hassabis, S. Velankar, *Nucleic Acids Res.* **2024**, *52*, D368.
- [53] F. Ahmadi, M. Simchi, J. M. Perry, S. Frenette, H. Benali, J.-P. Soucy, G. Massarweh, S. C. C. Shih, *Lab. Chip* **2022**, *23*, 81.
- [54] Ö. Üzuner, X. Zhang, T. Sibanda, *J. Am. Med. Inform. Assoc.* **2009**, *16*, 109.
- [55] S. Sette, L. Boullart, *Eng. Appl. Artif. Intell.* **2000**, *13*, 381.
- [56] L. Zhou, S. Pan, J. Wang, A. V. Vasilakos, *Neurocomputing* **2017**, *237*, 350.
- [57] O. Y. Al-Jarrah, P. D. Yoo, S. Muhaidat, G. K. Karagiannis, K. Taha, *Big Data Res.* **2015**, *2*, 87.
- [58] H. Tao, T. Wu, S. Kheiri, M. Aldeghi, A. Aspuru-Guzik, E. Kumacheva, *Adv. Funct. Mater.* **2021**, *31*, 2106725.
- [59] A. A. Volk, R. W. Epps, D. T. Yonemoto, B. S. Masters, F. N. Castellano, K. G. Reyes, M. Abolhasani, *Nat. Commun.* **2023**, *14*, 1403.
- [60] A. Lashkaripour, C. Rodriguez, N. Mehdipour, R. Mardian, D. McIntyre, L. Ortiz, J. Campbell, D. Densmore, *Nat. Commun.* **2021**, *12*, 25.
- [61] K. Gardner, M. M. Uddin, L. Tran, T. Pham, S. Vanapalli, W. Li, *Lab. Chip* **2022**, *22*, 4067.
- [62] H. Sun, W. Xie, J. Mo, Y. Huang, H. Dong, *Front. Bioeng. Biotechnol.* **2023**, *11*, 1208648.
- [63] R. Morizane, J. V. Bonventre, *Nat. Protoc.* **2017**, *12*, 195.
- [64] A. S. Monzel, K. Hemmer, T. Kaoma, L. M. Smits, S. Bolognin, P. Lucarelli, I. Rosety, A. Zagare, P. Antony, S. L. Nickels, R. Krueger, F. Azuaje, J. C. Schwaborn, *Parkinsonism Relat. Disord.* **2020**, *75*, 105.
- [65] M. Gantz, S. V. Mathis, F. E. H. Nintzel, P. Lio, F. Hollfelder, *Faraday Discuss.* **2024**, *252*, 89.
- [66] M. P. McRae, G. Simmons, J. Wong, J. T. McDevitt, *ACC. Chem. Res.* **2016**, *49*, 1359.
- [67] J. Riordon, D. Sovilj, S. Sanner, D. Sinton, E. W. K. Young, *Trends Biotechnol.* **2019**, *37*, 310.
- [68] D. McIntyre, A. Lashkaripour, P. Fordyce, D. Densmore, *Lab. Chip* **2022**, *22*, 2925.
- [69] M. Vasina, D. Kovar, J. Damborsky, Y. Ding, T. Yang, A. deMello, S. Mazurenko, S. Stavrakis, Z. Prokop, *Biotechnol. Adv.* **2023**, *66*, 108171.
- [70] X. Chen, H. Lv, *NPG Asia Mater.* **2022**, *14*, 1.
- [71] T. Moragues, D. Arguijo, T. Beneyton, C. Modavi, K. Simutis, A. R. Abate, J.-C. Baret, A. J. deMello, D. Densmore, A. D. Griffiths, *Nat. Rev. Methods Primer* **2023**, *3*, 1.
- [72] A. Samimi, S. Hengoju, M. A. Rosenbaum, *Sens. Actuators B Chem.* **2024**, *417*, 136162.
- [73] X. Cao, T. Buryška, T. Yang, J. Wang, P. Fischer, A. Streets, S. Stavrakis, A. deMello, *Lab. Chip* **2023**, *23*, 2029.
- [74] C. Holtze, A. C. Rowat, J. J. Agresti, J. B. Hutchison, F. E. Angilè, C. H. J. Schmitz, S. Köster, H. Duan, K. J. Humphry, R. A. Scanga, J. S. Johnson, D. Pisignano, D. A. Weitz, *Lab. Chip* **2008**, *8*, 1632.
- [75] M. T. Guo, A. Rotem, J. A. Heyman, D. A. Weitz, *Lab. Chip* **2012**, *12*, 2146.

- [76] Y. Ding, J. Choo, A. J. deMello, *Microfluid. Nanofluidics* **2017**, *21*, 58.
- [77] E. W. K. Young, D. J. Beebe, *Chem. Soc. Rev.* **2010**, *39*, 1036.
- [78] N. J. Carroll, S. B. Rathod, E. Derbins, S. Mendez, D. A. Weitz, D. N. Petsev, *Langmuir* **2008**, *24*, 658.
- [79] T. Moragues, S. Mitchell, D. F. Akl, J. Pérez-Ramírez, A. deMello, *Small Struct.* **2023**, *4*, 2200284.
- [80] Y. Du, J. Shim, M. Vidula, M. J. Hancock, E. Lo, B. G. Chung, J. T. Borenstein, M. Khabiry, D. M. Cropek, A. Khademhosseini, *Lab. Chip* **2009**, *9*, 761.
- [81] S. Sant, M. J. Hancock, J. P. Donnelly, D. Iyer, A. Khademhosseini, *Can. J. Chem. Eng.* **2010**, *88*, 899.
- [82] H. Song, R. F. Ismagilov, *J. Am. Chem. Soc.* **2003**, *125*, 14613.
- [83] G. Zheng, Y. Wang, J. Qin, *Anal. Bioanal. Chem.* **2012**, *404*, 3061.
- [84] Z. Wu, H. Yang, H. Xu, W. Dai, L. Xu, H. Du, D. Zhang, *Phys. Fluids* **2024**, *36*, 072014.
- [85] S.-J. Wang, W. Saadi, F. Lin, C. M.-C. Nguyen, N. L. Jeon, *Exp. Cell Res.* **2004**, *300*, 180.
- [86] A. V. Nguyen, M. Yaghoobi, M. Azizi, M. Davaritouchaee, K. W. Simpson, A. Abbaspourrad, *Commun. Eng.* **2023**, *2*, 1.
- [87] C.-W. Chang, Y.-J. Cheng, M. Tu, Y.-H. Chen, C.-C. Peng, W.-H. Liao, Y.-C. Tung, *Lab Chip* **2014**, *14*, 3762.
- [88] W. Du, L. Li, K. P. Nichols, R. F. Ismagilov, *Lab. Chip* **2009**, *9*, 2286.
- [89] Y. Li, J. Xuan, R. Hu, P. Zhang, X. Lou, Y. Yang, *Talanta* **2019**, *204*, 569.
- [90] Y.-C. Toh, T. C. Lim, D. Tai, G. Xiao, D. Van Noort, H. Yu, *Lab. Chip* **2009**, *9*, 2026.
- [91] X. Luo, J.-Y. Chen, M. Ataei, A. Lee, *Biosensors* **2022**, *12*, 58.
- [92] S. Rockel, M. Geertz, S. J. Maerkl, in *Gene Regulatory Networks: Methods and Protocols* (Eds: B. Deplancke, N. Gheldof), Humana Press, Totowa, NJ **2012**, pp. 97–114.
- [93] S. Mukherjee, M. F. Berger, G. Jona, X. S. Wang, D. Muzzey, M. Snyder, R. A. Young, M. L. Bulyk, *Nat. Genet.* **2004**, *36*, 1331.
- [94] C. Ponzetto, A. Bardelli, Z. Zhen, F. Maina, P. dalla Zonca, S. Giordano, A. Graziani, G. Panayotou, P. M. Comoglio, *Cell* **1994**, *77*, 261.
- [95] M. Geertz, D. Shore, S. J. Maerkl, *Proc. Natl. Acad. Sci.* **2012**, *109*, 16540.
- [96] Z. Yu, S. Lu, Y. Huang, *Anal. Chem.* **2014**, *86*, 9386.
- [97] H. van den Bos, D. C. J. Spierings, A. Taudt, B. Bakker, D. Porubský, E. Falconer, C. Novoa, N. Halsema, H. G. Kazemier, K. Hoekstra-Wakker, V. Guryev, W. F. A. den Dunnen, F. Fojier, M. Colomé-Tatché, H. W. G. M. Boddeke, P. M. Lansdorp, *Genome Biol.* **2016**, *17*, 116.
- [98] K. E. Szulwach, P. Chen, X. Wang, J. Wang, L. S. Weaver, M. L. Gonzales, G. Sun, M. A. Unger, R. Ramakrishnan, *PLoS One* **2015**, *10*, e0135007.
- [99] Y. Yang, J. F. Swennenhuis, H. S. Rho, S. L. Gac, L. W. M. M. Terstappen, *PLoS One* **2014**, *9*, e107958.
- [100] S. Srikanth, S. K. Dubey, A. Javed, S. Goel, *Sens. Actuators Phys.* **2021**, *332*, 113096.
- [101] V. Anagnostidis, B. Sherlock, J. Metz, P. Mair, F. Hollfelder, F. Gielen, *Lab. Chip* **2020**, *20*, 889.
- [102] K. Duncan, B. B. Doll, N. D. Daw, D. Shohamy, *Neuron* **2018**, *98*, 645.
- [103] O. J. Dressler, P. D. Howes, J. Choo, A. J. deMello, *ACS Omega* **2018**, *3*, 10084.
- [104] J. Vamathevan, D. Clark, P. Czodrowski, I. Dunham, E. Ferran, G. Lee, B. Li, A. Madabhushi, P. Shah, M. Spitzer, S. Zhao, *Nat. Rev. Drug Discov.* **2019**, *18*, 463.
- [105] T. Rodrigues, *Drug Discov. Today Technol.* **2019**, *32–33*, 3.
- [106] A. F. de Almeida, R. Moreira, T. Rodrigues, *Nat. Rev. Chem.* **2019**, *3*, 589.
- [107] S. Jain, E. Kotsampasakou, G. F. Ecker, *J. Comput. Aided Mol. Des.* **2018**, *32*, 583.
- [108] J.-M. Lu, H.-F. Wang, Q.-H. Guo, J.-W. Wang, T.-T. Li, K.-X. Chen, M.-T. Zhang, J.-B. Chen, Q.-N. Shi, Y. Huang, S.-W. Shi, G.-Y. Chen, J.-Z. Pan, Z. Lu, Q. Fang, *Nat. Commun.* **2024**, *15*, 8826.
- [109] J. M. Granda, L. Donina, V. Dragone, D.-L. Long, L. Cronin, *Nature* **2018**, *559*, 377.
- [110] D. A. Pensak, E. J. Corey, in *Computer-Assisted Organic Synthesis*, Vol. 61 (Eds: W. T. Wipke, W. J. Howe), ACS Symposium Series, American Chemical Society, Washington, DC **1977**, pp. 1–32.
- [111] E. J. Corey, W. J. Howe, D. A. Pensak, *J. Am. Chem. Soc.* **1974**, *96*, 7724.
- [112] E. J. Corey, W. J. Howe, H. W. Orf, D. A. Pensak, G. Petersson, *J. Am. Chem. Soc.* **1975**, *97*, 6116.
- [113] J. Nette, P. D. Howes, A. J. deMello, *Adv. Mater. Technol.* **2020**, *5*, 2000060.
- [114] S. Krishnadasan, R. J. C. Brown, A. J. deMello, J. C. deMello, *Lab. Chip* **2007**, *7*, 1434.
- [115] L. Bezinge, R. M. Maceiczky, I. Lignos, M. V. Kovalenko, A. J. deMello, *ACS Appl. Mater. Interfaces* **2018**, *10*, 18869.
- [116] C. Dewi, R.-C. Chen, *Int. J. Innov. Comput. Inf. Control* **2019**, *15*, 2027.
- [117] R. W. Epps, M. S. Bowen, A. A. Volk, K. Abdel-Latif, S. Han, K. G. Reyes, A. Amassian, M. Abolhasani, *Adv. Mater.* **2020**, *32*, 2001626.
- [118] K. M. Tibbetts, X.-J. Feng, H. Rabitz, *Phys. Chem. Chem. Phys.* **2017**, *19*, 4266.
- [119] H. Liu, Y.-S. Ong, X. Shen, J. Cai, *IEEE Trans. Neural Netw. Learn. Syst.* **2020**, *31*, 4405.
- [120] Y. Song, Y. Jeong, T. Kwon, D. Lee, D. Y. Oh, T.-J. Park, J. Kim, J. Kim, S. Kwon, *Lab. Chip* **2017**, *17*, 429.
- [121] F. He, M.-J. Zhang, W. Wang, Q.-W. Cai, Y.-Y. Su, Z. Liu, Y. Faraj, X.-J. Ju, R. Xie, L.-Y. Chu, *Adv. Mater. Technol.* **2019**, *4*, 1800687.
- [122] T. Lin, Z. Wang, W. Wang, Y. Sui, *Soft Matter* **2021**, *17*, 4027.
- [123] S. A. Damiani, D. Rossi, H. N. Joensson, S. Damiani, *Sci. Rep.* **2020**, *10*, 19517.
- [124] Z. Su, J. He, P. Zhou, L. Huang, J. Zhou, *Lab. Chip* **2020**, *20*, 1907.
- [125] A. J. deMello, *Nature* **2006**, *442*, 394.
- [126] C. J. Taylor, A. Pomberger, K. C. Felton, R. Grainger, M. Barecka, T. W. Chamberlain, R. A. Bourne, C. N. Johnson, A. A. Lapkin, *Chem. Rev.* **2023**, *123*, 3089.
- [127] N. Hansen, in *New Evol. Comput. Adv. Estim. Distrib. Algorithms* (Eds: J. A. Lozano, P. Larrañaga, I. Inza, E. Bengoetxea), Springer, Berlin, Heidelberg **2006**, pp. 75–102.
- [128] B. A. Rizkin, A. S. Shkolnik, N. J. Ferraro, R. L. Hartman, *Nat. Mach. Intell.* **2020**, *2*, 200.
- [129] J. H. Jerman, S. C. Terry, *Environ. Int.* **1981**, *5*, 77.
- [130] A. T. Woolley, R. A. Mathies, *Proc. Natl. Acad. Sci.* **1994**, *91*, 11348.
- [131] A. Reece, B. Xia, Z. Jiang, B. Noren, R. McBride, J. Oakey, *Curr. Opin. Biotechnol.* **2016**, *40*, 90.
- [132] A. Mencattini, D. Di Giuseppe, M. C. Comes, P. Casti, F. Corsi, F. R. Bertani, L. Ghibelli, L. Businaro, C. Di Natale, M. C. Parrini, E. Martinelli, *Sci. Rep.* **2020**, *10*, 7653.
- [133] M. Sesen, G. Whyte, *Sci. Rep.* **2020**, *10*, 8736.
- [134] Y. Gu, A. C. Zhang, Y. Han, J. Li, C. Chen, Y.-H. Lo, *Cytometry A* **2019**, *95*, 499.
- [135] A. Jain, M. Teshima, T. Buryska, D. Romeis, M. Haslbeck, M. Döring, V. Sieber, S. Stavrakis, A. De Mello, *Angew. Chem.* **2024**, *136*, e202409610.
- [136] E. Huang, Y. Wang, D. Cai, D. Liu, *Interdiscip. Med.* **2024**, *2*, e20230026.
- [137] H. Zhao, Y. Zhang, D. Hua, *Micromachines* **2024**, *15*, 893.
- [138] J. Sun, W. Liu, Y. Li, A. Gholamipour-Shirazi, A. Abdulla, X. Ding, *Microfluid. Nanofluidics* **2017**, *21*, 125.
- [139] C. M. Leung, P. de Haan, K. Ronaldson-Bouchard, G.-A. Kim, J. Ko, H. S. Rho, Z. Chen, P. Habibovic, N. L. Jeon, S. Takayama, M. L. Shuler, G. Vunjak-Novakovic, O. Frey, E. Verpoorte, Y.-C. Toh, *Nat. Rev. Methods Primer* **2022**, *2*, 1.
- [140] M. Dai, G. Xiao, M. Shao, Y. S. Zhang, *Biosensors* **2023**, *13*, 389.
- [141] L. Wang, J. Han, W. Su, A. Li, W. Zhang, H. Li, H. Hu, W. Song, C. Xu, J. Chen, *Microsyst. Nanoeng.* **2023**, *9*, 1.
- [142] D. Huh, B. D. Matthews, A. Mammoto, M. Montoya-Zavala, H. Y. Hsin, D. E. Ingber, *Science* **2010**, *328*, 1662.
- [143] G. Holzner, B. Mateescu, D. van Leeuwen, G. Cereghetti, R. Dechant, S. Stavrakis, A. deMello, *Cell Rep.* **2021**, *34*, 108824.
- [144] A. S. Rane, J. Rutkauskaitė, A. deMello, S. Stavrakis, *Chem* **2017**, *3*, 588.
- [145] M. Doan, A. E. Carpenter, *Nat. Mater.* **2019**, *18*, 414.
- [146] B. Poschkamp, S. Bekešchus, *Cytometry A* **2024**, *105*, 356.
- [147] T. E. Hybel, S. H. Jensen, M. A. Rodrigues, T. E. Hybel, M. N. Pedersen, S. H. Qvick, M. H. Enemark, M. Bill, C. A. Rosenberg, M. Ludvigsen, *Int. J. Mol. Sci.* **2024**, *25*, 6465.
- [148] S. Zhou, B. Chen, E. S. Fu, H. Yan, *Microsyst. Nanoeng.* **2023**, *9*, 1.
- [149] C. F. Oteşteanu, M. Ugrinic, G. Holzner, Y.-T. Chang, C. Fassnacht, E. Guenova, S. Stavrakis, A. deMello, M. Claassen, *Cell Rep. Methods* **2021**, *1*, 100094.
- [150] E. Zang, S. Brandes, M. Tovar, K. Martin, F. Mech, P. Horbert, T. Henkel, M. T. Figge, M. Roth, *Lab. Chip* **2013**, *13*, 3707.
- [151] A. Isozaki, H. Mikami, H. Tezuka, H. Matsumura, K. Huang, M. Akamie, K. Hiramatsu, T. Iino, T. Ito, H. Karakawa, Y. Kasai, Y. Li, Y. Nakagawa, S. Ohnuki, T. Ota, Y. Qian, S. Sakuma, T. Sekiya, Y. Shirasaki, N. Suzuki, E. Tayyabi, T. Wakamiya, M. Xu, M. Yamagishi, H. Yan, Q. Yu, S. Yan, D. Yuan, W. Zhang, et al., *Lab. Chip* **2020**, *20*, 2263.
- [152] L. Howell, V. Anagnostidis, F. Gielen, *Adv. Mater. Technol.* **2022**, *7*, 2101053.
- [153] G. Soldati, F. D. Ben, G. Brisotto, E. Biscontin, M. Bulfoni, A. Piruska, A. Steffan, M. Turetta, V. D. Mea, *Am. J. Transl. Res.* **2018**, *10*, 4004.
- [154] S. Sarkar, W. Kang, S. Jiang, K. Li, S. Ray, E. Luther, A. R. Ivanov, Y. Fu, T. Konry, *Lab. Chip* **2020**, *20*, 2317.
- [155] M. Kapalczyńska, T. Kolenda, W. Przybyła, M. Zajączkowska, A. Teresiak, V. Filas, M. Ibbes, R. Bliźniak, Ł. Łuczewski, K. Lamperska, *Arch. Med. Sci. AMS* **2018**, *14*, 910.
- [156] J. Li, J. Chen, H. Bai, H. Wang, S. Hao, Y. Ding, B. Peng, J. Zhang, L. Li, W. Huang, *Research* **2022**, *2022*, 9869518.

- [157] B. P. Jena, D. L. Gatti, S. Arslanturk, S. Pernal, D. J. Taatjes, *Micron* **2019**, *117*, 55.
- [158] S. Han, T. Kim, D. Kim, Y.-L. Park, S. Jo, *IEEE Robot. Autom. Lett.* **2018**, *3*, 873.
- [159] D. Huh, H. Fujioka, Y.-C. Tung, N. Futai, R. Paine, J. B. Grotberg, S. Takayama, *Proc. Natl. Acad. Sci.* **2007**, *104*, 18886.
- [160] S. Lee, J. Ko, D. Park, S.-R. Lee, M. Chung, Y. Lee, N. L. Jeon, *Lab. Chip* **2018**, *18*, 2686.
- [161] S. Deng, C. Li, J. Cao, Z. Cui, J. Du, Z. Fu, H. Yang, P. Chen, *Theranostics* **2023**, *13*, 4526.
- [162] J. J. Tronolone, T. Mathur, C. P. Chafdari, A. Jain, *Ann. Biomed. Eng.* **2023**, *51*, 1723.
- [163] S. Parlato, A. De Ninno, R. Molfetta, E. Toschi, D. Salerno, A. Mencattini, G. Romagnoli, A. Fragale, L. Roccazzello, M. Buoncervello, I. Canini, E. Bentivegna, M. Falchi, F. R. Bertani, A. Gerardino, E. Martinelli, C. Natale, R. Paolini, L. Businaro, L. Gabriele, *Sci. Rep.* **2017**, *7*, 1093.
- [164] J. Li, J. Chen, H. Bai, H. Wang, S. Hao, Y. Ding, B. Peng, J. Zhang, L. Li, W. Huang, *Research* **2022**, *2022*, 9869518.
- [165] M. A. A. Baig, D. S. Li, in *2024 8th Asian Conf. on Artificial Intelligence Technology (ACAIT)*, IEEE, USA **2024**, pp. 297–306, <https://doi.org/10.31224/3876>.
- [166] S. Battat, D. A. Weitz, G. M. Whitesides, *Lab. Chip* **2022**, *22*, 530.
- [167] J. Park, Y. W. Kim, H.-J. Jeon, *Biosensors* **2024**, *14*, 613.
- [168] H. Amini, E. Sollier, M. Masaali, Y. Xie, B. Ganapathysubramanian, H. A. Stone, D. Di Carlo, *Nat. Commun.* **2013**, *4*, 1826.
- [169] D. Stoecklein, C.-Y. Wu, K. Owsley, Y. Xie, D. D. Carlo, B. Ganapathysubramanian, *Lab. Chip* **2014**, *14*, 4197.
- [170] K. S. Paulsen, D. Di Carlo, A. J. Chung, *Nat. Commun.* **2015**, *6*, 6976.
- [171] J. K. Nunes, C.-Y. Wu, H. Amini, K. Owsley, D. Di Carlo, H. A. Stone, *Adv. Mater.* **2014**, *26*, 3712.
- [172] E. Sollier, H. Amini, D. E. Go, P. A. Sandoz, K. Owsley, D. Di Carlo, *Microfluid. Nanofluidics* **2015**, *19*, 53.
- [173] D. Stoecklein, K. G. Lore, M. Davies, S. Sarkar, B. Ganapathysubramanian, *Sci. Rep.* **2017**, *7*, 46368.
- [174] F. D. M. Neto, A. J. Da Silva Neto, *An Introduction to Inverse Problems with Applications*, Springer, Berlin, Heidelberg **2013**.
- [175] V. Mnih, K. Kavukcuoglu, D. Silver, A. Graves, I. Antonoglou, D. Wierstra, M. Riedmiller, *IEEE Trans. Pattern Anal. Mach. Intell.* **2013**, *35*, 2206.
- [176] C. Blundell, B. Uria, A. Pritzel, Y. Li, A. Ruderman, J. Z. Leibo, J. Rae, D. Wierstra, D. Hassabis (Preprint), arXiv:1606.04460, Submitted Jun. **2016**.
- [177] J. W. Khor, N. Jean, E. S. Luxenberg, S. Ermon, S. K. Y. Tang, *Soft Matter* **2019**, *15*, 1361.
- [178] M. Durve, F. Bonaccorso, A. Montessori, M. Lauricella, A. Tiribocchi, S. Succi, *Philos. Trans. R. Soc. Math. Phys. Eng. Sci.* **2021**, *379*, 20200400.
- [179] P. Hadikhani, N. Borhani, S. M. H. Hashemi, D. Psaltis, *Sci. Rep.* **2019**, *9*, 8114.
- [180] J. Redmon, S. Divvala, R. Girshick, A. Farhadi, in *2016 IEEE Conf. on Computer Vision and Pattern Recognition (CVPR)* **2016**, p. 779.
- [181] W. Liu, D. Anguelov, D. Erhan, C. Szegedy, S. Reed, C.-Y. Fu, A. C. Berg, in *B. Leibe, J. Matas, N. Sebe, M. Welling, in Computer Vision—ECCV 2016 (Eds: B. Leibe, J. Matas, N. Sebe, M. Welling)*, Springer International Publishing, Cham **2016**, pp. 21–37.
- [182] A. Chu, D. Nguyen, S. S. Talathi, A. C. Wilson, C. Ye, W. L. Smith, A. D. Kaplan, E. B. Duoss, J. K. Stolaroff, B. Giera, *Lab. Chip* **2019**, *19*, 1808.
- [183] E. E. Tsur, *Annu. Rev. Biomed. Eng.* **2020**, *22*, 285.
- [184] J. W. Hong, S. R. Quake, *Nat. Biotechnol.* **2003**, *21*, 1179.
- [185] N. Amin, W. Thies, S. Amarasinghe, in *2009 IEEE Int. Conf. on Computer Design, IEEE, Lake Tahoe, CA* **2009**, pp. 2–9.
- [186] H. Huang, D. Densmore, *ACM J. Emerg. Technol. Comput. Syst.* **2014**, *11*, 1.
- [187] T.-M. Tseng, M. Li, B. Li, T.-Y. Ho, U. Schlichtmann, in *Proc. of the 53rd Annual Design Automation Conf., Association For Computing Machinery, New York, NY* **2016**, pp. 1–6.
- [188] R. Sanka, J. Lippai, D. Samarasekera, S. Nemsick, D. Densmore, *Sci. Rep.* **2019**, *9*, 9166.
- [189] B. Mosadegh, T. Bersano-Begey, J. Y. Park, M. A. Burns, S. Takayama, *Lab. Chip* **2011**, *11*, 2813.
- [190] L. W. Nagel, D. O. Pederson, in *16th Midwest Symp. on Circuit Theory, Waterloo, ON* **1973**, UCB/ERL M382, <https://www2.eecs.berkeley.edu/Pubs/TechRpts/1973/22871.html>.
- [191] F. Su, K. Chakrabarty, R. B. Fair, *IEEE Trans. Comput.-Aided Des. Integr. Circuits Syst.* **2006**, *25*, 211.
- [192] W. Thies, J. P. Urbanski, T. Thorsen, S. Amarasinghe, *Nat. Comput.* **2008**, *7*, 255.
- [193] A. M. Amin, M. Thottethodi, T. N. Vijaykumar, S. Wereley, S. C. Jacobson, *SIGARCH Comput. Arch. News* **2007**, *35*, 254.
- [194] L. Ruddigkeit, R. van Deursen, L. C. Blum, J.-L. Reymond, *J. Chem. Inf. Model.* **2012**, *52*, 2864.
- [195] I. V. Tetko, O. Engkvist, U. Koch, J.-L. Reymond, H. Chen, *Mol. Inform.* **2016**, *35*, 615.
- [196] G. Hinton, O. Vinyals, J. Dean (Preprint), arXiv:1503.02531, v1, Submitted: Mar. **2015**.
- [197] J. Zhou, G. Cui, S. Hu, Z. Zhang, C. Yang, Z. Liu, L. Wang, C. Li, M. Sun, *AI Open* **2020**, *1*, 57.
- [198] I. Shashkov, A. Zaytsev, N. Balabin, E. Burnaev, in *Proc. of the 2022 5th Int. Conf. on Artificial Intelligence and Pattern Recognition 2022*, pp. 8–13, **2022**.
- [199] M. Roberts, D. Driggs, M. Thorpe, J. Gilbey, M. Yeung, S. Ursprung, A. I. Aviles-Rivero, C. Etmann, C. McCague, L. Beer, J. R. Weir-McCall, Z. Teng, E. Gkrania-Klotsas, J. H. F. Rudd, E. Sala, C.-B. Schönlieb, *Nat. Mach. Intell.* **2021**, *3*, 199.
- [200] Agilent, *2100 Bioanalyzer Instrument*, <https://www.agilent.com/en/product/automated-electrophoresis/bioanalyzer-systems/bioanalyzer-instrument/2100-bioanalyzer-instrument-228250> (accessed: April 5, 2025).
- [201] A. Stephenson, L. Lastra, B. Nguyen, Y.-J. Chen, J. Nivala, L. Ceze, K. Strauss, *ACS Synth. Biol.* **2023**, *12*, 3156.
- [202] *Bio-Rad's Droplet Digital PCR*, <https://www.bio-rad.com/en-ch/category/digital-pcr?ID=bcdf1371-fa15-9804-647b-4c13f34cd622> (accessed: April 18, 2025).
- [203] K. Robison, *Omicst! Omicst!*, <https://omicstomics.blogspot.com/> (accessed: April 29, 2025).
- [204] N. Hillson, M. Caddick, Y. Cai, J. A. Carrasco, M. W. Chang, N. C. Curach, D. J. Bell, R. L. Feuvre, D. C. Friedman, X. Fu, N. D. Gold, M. J. Herggård, M. B. Holowko, J. R. Johnson, R. A. Johnson, J. D. Keasling, R. I. Kitney, A. Kondo, C. Liu, V. J. J. Martin, F. Menolascina, C. Ogino, N. J. Patron, M. Pavan, C. L. Poh, I. S. Pretorius, S. J. Rosser, N. S. Scrutton, M. Storch, et al., *Nat. Commun.* **2019**, *10*, 2040.
- [205] D. Juchli, S. Beutel, F. Lenk, in *Smart Biolabs Future* (Eds: S. Beutel, F. Lenk), Springer International Publishing, Cham **2022**, pp. 147–174.
- [206] L. Bromig, D. Leiter, A.-V. Mardale, N. von den Eichen, E. Bieringer, D. Weuster-Botz, *SoftwareX* **2022**, *17*, 100991.
- [207] C. Arnold, *Nature* **2022**, *606*, 612.
- [208] T. Evans, C. O. Retzlaff, C. Geißler, M. Kargl, M. Plass, H. Müller, T.-R. Kiehl, N. Zerbe, A. Holzinger, *Future Gener. Comput. Syst.* **2022**, *133*, 281.
- [209] R. Dwivedi, D. Dave, H. Naik, S. Singhal, R. Omer, P. Patel, B. Qian, Z. Wen, T. Shah, G. Morgan, R. Ranjan, *ACM Comput. Surv.* **2023**, *55*, 194, 1.
- [210] *Artificial Intelligence and Machine Learning in Software as a Medical Device*, <https://www.fda.gov/medical-devices/software-medical-device-samd/artificial-intelligence-software-medical-device> (accessed: May 5, 2025).
- [211] N. Banaei, J. Moshfegh, A. Mohseni-Kabir, J. M. Houghton, Y. Sun, B. Kim, *RSC Adv.* **2019**, *9*, 1859.
- [212] J. Zheng, T. Cole, Y. Zhang, J. Kim, S.-Y. Tang, *Biosens. Bioelectron.* **2021**, *194*, 113666.
- [213] P. Desir, T.-Y. Chen, M. Bracconi, B. Saha, M. Maestri, D. G. Vlachos, *React. Chem. Eng.* **2019**, *5*, 39.
- [214] M. S. Manak, J. S. Varsanik, B. J. Hogan, M. J. Whitfield, W. R. Su, N. Joshi, N. Steinke, A. Min, D. Berger, R. J. Saphirstein, G. Dixit, T. Meyyappan, H.-M. Chu, K. B. Knopf, D. M. Albalá, G. R. Sant, A. C. Chander, *Nat. Biomed. Eng.* **2018**, *2*, 761.
- [215] M. Shayan, S. Bhattacharjee, Y.-A. Song, K. Chakrabarty, R. Karri, *IEEE Trans. Very Large Scale Integr. VLSI Syst.* **2019**, *27*, 2755.
- [216] M. T. Doganay, P. Chakrabarty, S. M. Bommakanti, S. Jammalamadaka, D. Battalapalli, A. Madabhushi, M. S. Draz, *Lab. Chip* **2024**, *24*, 4998.
- [217] P. Changpetch, A. Pitpeng, S. Hiriotte, C. Yuangyai, *Computation* **2021**, *9*, 99.
- [218] I. Kundacina, O. Kundacina, D. Miskovic, V. Radonic, *Lab. Chip* **2025**, *25*, 657.

Manuscript received: May 22, 2025

Revised manuscript received: July 10, 2025

Version of record online: